

## Information Sciences

Special Topic: Novel Optoelectronic Devices

**Integrated optoelectronics with two-dimensional materials**Zhenzhou Cheng<sup>1,2,\*</sup>, Rongxiang Guo<sup>1,2</sup>, Jiaqi Wang<sup>3,\*</sup>, Yi Wang<sup>4</sup>, Zhengkun Xing<sup>1,2</sup>, Lei Ma<sup>1,5</sup>, Wei Wei<sup>6,7</sup>, Yu Yu<sup>8,9,\*</sup>, Hon Ki Tsang<sup>4,\*</sup> & Tiegeng Liu<sup>1,2</sup><sup>1</sup> School of Precision Instruments and Optoelectronics Engineering, Tianjin University, Tianjin 300072, China;<sup>2</sup> Key Laboratory of Optoelectronics Information Technology, Ministry of Education, Tianjin 300072, China;<sup>3</sup> College of Physics and Optoelectronic Engineering, Shenzhen University, Shenzhen 518060, China;<sup>4</sup> Department of Electronic Engineering, The Chinese University of Hong Kong, Hong Kong 999077, China;<sup>5</sup> Tianjin International Center for Nanoparticles and Nanosystems, Tianjin University, Tianjin 300072, China;<sup>6</sup> College of Optoelectronic Engineering, Chongqing University, Chongqing 400044, China;<sup>7</sup> Key Laboratory of Optoelectronic Technology and System, Ministry of Education, Chongqing 400044, China;<sup>8</sup> Wuhan National Laboratory for Optoelectronics, Wuhan 430074, China;<sup>9</sup> School of Optical and Electronic Information, Huazhong University of Science and Technology, Wuhan 430074, China\*Corresponding authors (emails: [zhenzhoucheng@tju.edu.cn](mailto:zhenzhoucheng@tju.edu.cn) (Zhenzhou Cheng); [jqwang@szu.edu.cn](mailto:jqwang@szu.edu.cn) (Jiaqi Wang); [yuyu@mail.hust.edu.cn](mailto:yuyu@mail.hust.edu.cn) (Yu Yu); [hktsang@ee.cuhk.edu.hk](mailto:hktsang@ee.cuhk.edu.hk) (Hon Ki Tsang))

Received 31 March 2022; Revised 10 May 2022; Accepted 25 May 2022; Published online 27 October 2022

**Abstract:** As we enter the post-Moore era, heterogeneous optoelectronic integrated circuits (OEICs) are attracting significant attention as an alternative approach to scaling to smaller-sized transistors. Two-dimensional (2D) materials, offering a range of intriguing optoelectronic properties as semiconductors, semimetals, and insulators, provide great potential for developing next-generation heterogeneous OEICs. For instance, Fermi levels of 2D materials can be tuned by applying electrical voltages, while their atomically thin geometries are inherently suited for the fabrication of planar devices without suffering from lattice mismatch. Since the first graphene-on-silicon OEICs were demonstrated in 2011, 2D-material heterogeneous OEICs have significantly progressed. To date, researchers have a better understanding of the importance of interface states on the optical properties of chip-integrated 2D materials. Moreover, there has been impressive progress towards the use of 2D materials for waveguide-integrated lasers, modulators, and photodetectors. In this review, we summarize the history, status, and trend of integrated optoelectronics with 2D materials.

**Keywords:** integrated optoelectronics, two-dimensional materials, heterogeneous integration, silicon photonics

**Introduction**

With entering the post-Moore era, information and communications technology (ICT) cannot enjoy the free ride of the fast growth of performance through simply shrinking transistor footprints, such that the optoelectronic integration starts to receive much more attention for building up new chip architectures [1]. By elaborately designing and integrating photonic and electronic devices monolithically on a chip, optoelectronic integrated circuits (OEICs) are expected to enable high-speed and stable signal sensing [2,3], pro-

cessing [4–6], and communications [7,8] in many application scenarios with the merits of small device footprints, inexpensive unit costs, and low energy dissipation. Since the concept of integrated optics was first proposed by Miller [9] in 1964, integrated optoelectronics undergoes expeditious evolution for more than half a century together with the rapid development of the semiconductor industry. Nowadays numerous material platforms, such as silicon and its compounds [10,11], germanium [12,13], gallium arsenide [14], indium phosphide (InP) [15], and lithium niobate ( $\text{LiNbO}_3$ ) [16,17], have been widely explored to develop OEICs. Different from microelectronic integrated circuits (ICs), which are typically built on silicon wafers, it is challenging to achieve diverse optoelectronic functions, such as light generation, guidance, modulation, and photodetection, in a single material platform, due to intrinsic limitations of materials' energy band structures. Consequently, heterogeneous integration [18–22] has been known as a feasible strategy for promoting the advancement of OEICs in the past decades.

Among current semiconducting materials, two-dimensional (2D) materials, a type of emerging atomically thin materials, have drawn intense research interest in the development of heterogeneous integration in recent years. Compared with bulk materials, 2D materials have superior advantages of electrical tunability of Fermi levels due to their low carrier densities [23], intrinsic compatibility to the fabrication of planar devices, and moderate requirements of the lattice match for heterostructure integration due to the weak van der Waals interaction between adjacent layers [24]. After the first 2D material, namely graphene, was experimentally isolated from bulk graphite [23] and epitaxially grown on silicon carbide substrates [25], the 2D material family has rapidly expanded to hundreds of examples [26], such as hexagonal boron nitride [27], transition metal dichalcogenides (TMDs) [28], black phosphorus (BP) [29], and Xenex [30], with an extensive range of intriguing optoelectronic properties. Until 2011, the first waveguide-integrated electro-optical modulator with a 1-GHz bandwidth was experimentally demonstrated based on graphene-on-silicon OEICs [31]. In this study, the waveguide-integrated device structure significantly enhances graphene's absorption of the propagating light in the silicon waveguide via the in-plane evanescent-field coupling configuration without modifying graphene's energy band structure, which overcomes the limitation of the moderate light-matter interaction in 2D-material devices [23]. Since then, the work has opened a new avenue toward the study of 2D-material heterogeneous integrated optoelectronics. To date, OEICs have been extensively investigated with the versatile combination of optical waveguide devices and 2D materials, as schematically shown in Figure 1, to boost the performance of conventional optoelectronic devices.

In this review, we comprehensively review the history, status, and trend of integrated optoelectronics with 2D materials. Specifically, in Section “Optoelectronic properties of 2D materials with IR photon responses”, we discuss optoelectronic properties of the 2D materials whose photon responses cover the infrared (IR) wavelength region including graphene, BP,  $\text{MoTe}_2$ ,  $\text{PtSe}_2$ , and  $\text{PdSe}_2$ . In Section “Fabrication of 2D-material heterogeneous OEICs”, we introduce fabrication methods of 2D-material heterogeneous OEICs. In Section “Light-matter interaction in 2D-material hybrid optical waveguides”, we focus on the studies of the light-matter interaction in waveguide-integrated 2D-material devices. In Sections “On-chip 2D-material lasers”, “On-chip 2D-material electro-optical modulators”, and “On-chip 2D-material photodetectors”, we review the studies of waveguide-integrated 2D-material optoelectronic devices, namely, on-chip lasers, electro-optical modulators, and photodetectors. In Section “Summary and prospect”, we summarize the review and discuss the prospect. Readers can gain basic knowledge, state-of-the-art techniques, and cutting-edge advances in integrated optoelectronics with 2D materials through reading this review.

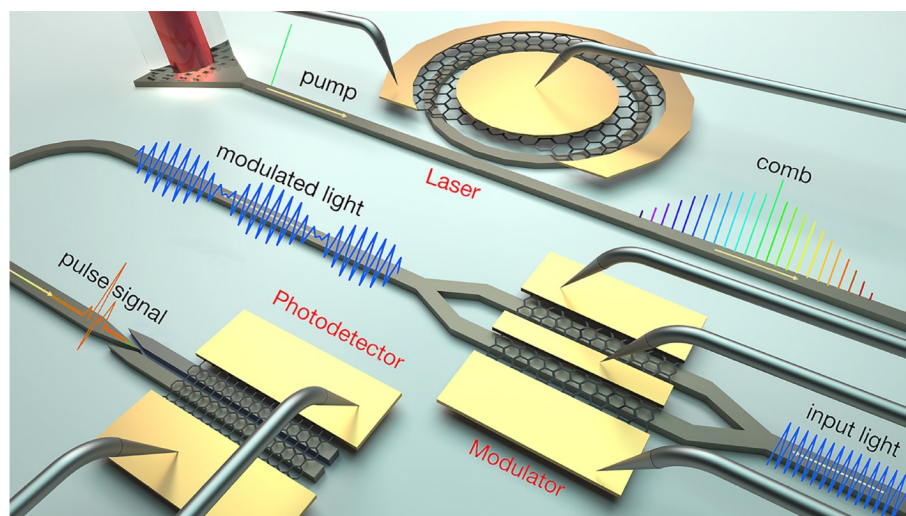


**Figure 1** Schematic of the proposed 2D-material heterogeneous OEICs. By integrating 2D materials on optical waveguides, innovative optoelectronic devices, namely, lasers, modulators, and photodetectors, with high performance and low power consumption, can be developed monolithically on a chip, serving as a powerful platform for the ICT development in the post-Moore era.

## Optoelectronic properties of 2D materials with IR photon responses

Due to the incomparable advantages of IR photonics, on-chip IR optoelectronic applications have attracted great attention, which may be divided into distinct spectral ranges, namely near-IR (0.75–1  $\mu\text{m}$ ), short/mid/long-wave IR (1–15  $\mu\text{m}$ ), and far-IR (15–100  $\mu\text{m}$ ) wavelengths. Among the discovered 2D materials, graphene, BP, and a portion of TMDs (e.g.,  $\text{MoTe}_2$ ,  $\text{PtSe}_2$ , and  $\text{PdSe}_2$ ) have excellent photon responsivity at IR wavelengths. Therefore, in this section, we mainly focus on the discussion of optoelectronic properties of the above 2D materials.

Graphene, which consists of a single layer of carbon atoms arranged in a honeycomb lattice, is the first discovered 2D material. Even though the theoretical investigation of graphene began as early as 1947 [32], it was experimentally discovered until 2004 [23,25]. As the conduction and valence bands of graphene touch each other at six points, known as Dirac points, in the momentum space, graphene, thus, exhibits an ultrawide spectral response region covering from visible light to terahertz frequencies. Previous studies show that there is a linear relation between the number of layers and the transmittance of a graphene sheet, with about 2.3% absorption of the vertically incident illumination for the single-layer material [33]. Nowadays, the carrier mobility of graphene could be as high as  $200,000 \text{ cm}^2/(\text{V s})$  [34] at room temperature, which is more than 100 times higher than that of silicon. Besides, graphene was measured to possess a giant nonlinear refractive index (RI) of  $\sim 10^{-11} \text{ m}^2/\text{W}$ , almost nine orders of magnitude larger than bulk dielectrics [35]. As a result, it is promising to develop ultra-fast optoelectronic devices and nonlinear optical devices based on graphene. However, the lack of a bandgap seriously affects graphene's applications to some extent since some devices are required to have high on/off ratios, namely field-effect transistors (FETs). Therefore, many studies focus on the bandgap engineering of graphene by using various approaches, such as multilayer stacking [36], chemical doping [37], or morphological tailoring [38].

Similar to graphene, BP is another type of 2D materials, which is composed of sheets with phosphorus

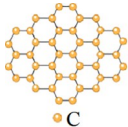
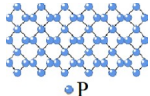
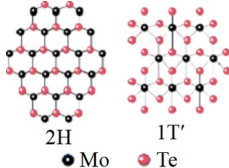
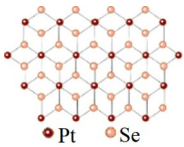
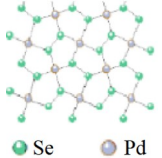
atoms arranged in a puckered honeycomb lattice. In 2014, Li *et al.* [29] demonstrated the first FET based on few-layer BP crystals with a carrier mobility as high as  $1000 \text{ cm}^2/(\text{V s})$  and a high on/off ratio of  $10^5$ . Compared with graphene, the bandgap of BP varies from 0.3 eV for bulk materials to 2.0 eV for monolayer BP sheets [39], indicating that the material can absorb light ranging from visible light to mid-IR wavelengths by adjusting the number of stacking BP layers. Later, Long *et al.* [40] demonstrated the impressive hole mobility of around  $45,000 \text{ cm}^2/(\text{V s})$  of BP at cryogenic temperatures, making it suitable for developing ultrafast optoelectronic devices. Besides, the previous study also revealed a range of anisotropic behaviors of BP [41], which could be used for detecting polarized light [42]. Moreover, the nonlinear RI of BP nanoplatelets was measured as  $\sim 6.8 \times 10^{-13} \text{ m}^2/\text{W}$  by a Z-scanning method [43]. Although BP exhibits the above intriguing optoelectronic and nonlinear optical characteristics, it normally suffers from poor chemical and physical stability [44]. Consequently, the material has to be protected to avoid degradation during practical applications [45].

Different from graphene and BP, TMDs refer to a branch of 2D materials with the chemical composition formula of  $\text{MX}_2$ , where  $\text{M} = \text{Ti, Zr, Hf, V, Nb, Ta, Cr, Mo, W, Pt, Pd}$ , and  $\text{X} = \text{S, Se, Te}$  [46]. Among the current TMDs,  $\text{MoTe}_2$ ,  $\text{PtSe}_2$ , and  $\text{PdSe}_2$  were demonstrated to have the potential to develop IR optoelectronic and nonlinear optical devices. As for  $\text{MoTe}_2$ , the material can exist in two crystal phases, namely, tripartite cylindrical and octahedral structures, which could be transformed between each other under certain conditions [47]. In 2017, Wang *et al.* [48] demonstrated the structural phase transition in a monolayer  $\text{MoTe}_2$  sheet for the first time. Also, by varying the thickness of  $\text{MoTe}_2$ , the bandgap of  $\text{MoTe}_2$  could gradually change due to the existence of the quantum constraint effect [47]. With the monolayer thickness,  $\text{MoTe}_2$  converts into a direct bandgap semiconductor with a bandgap of around 1.1 eV. On the other hand, layered  $\text{PtSe}_2$  and  $\text{PdSe}_2$  have been recently investigated for developing optoelectronic devices for long wavelengths. In 2015, Wang *et al.* [49] fabricated high-quality, single-crystalline, monolayer-thickness  $\text{PtSe}_2$  films in which the first-principle theoretic calculations revealed that the bandgap of the material is 1.2 eV. While, Sun *et al.* [50] investigated optoelectronic properties of monolayer  $\text{PdSe}_2$  by using first-principle calculations, indicating that  $\text{PdSe}_2$  exhibits typical semiconductor properties with an indirect bandgap of 0.03 eV for bulk and 1.43 eV for monolayer. Later, a monolayer  $\text{PdSe}_2$  sheet was experimentally demonstrated [51], which opened a door to the development of IR optoelectronic devices based on  $\text{PdSe}_2$ . It is worth noting that the carrier scattering and heavy effective mass normally make the carrier mobility of TMDs relatively low, which may be improved by using chemical doping approaches [52]. Besides the excellent optoelectronic properties, TMDs also have strong Kerr nonlinearity, namely, a nonlinear RI of  $\sim 10^{-15} \text{ m}^2/\text{W}$  for  $\text{PdSe}_2$  [53], which is about two orders of magnitude larger than bulk silicon. The comparison of the 2D materials with IR photon responses is summarized in Table 1.

## Fabrication of 2D-material heterogeneous OEICs

Since graphene was mechanically exfoliated from graphite in 2004 [23], various methods have been developed to prepare low-dimensional materials with atomic monolayer or multiple-layer thicknesses, such as chemical vapor deposition (CVD) growth [62], epitaxial growth [63], mechanically or chemically exfoliating [64], solution assembly [65], and chemical synthesis [66] methods. Taking the graphene preparation as an

**Table 1** Comparison of the 2D materials with IR photon responses

Material	Structure schematic	Material bandgap (eV)	Carrier mobility (cm <sup>2</sup> /Vs)	Material thickness (nm)	Optical absorption (%)	Nonlinear RI (m <sup>2</sup> /W)
Graphene		0 [23]	2.0×10 <sup>5</sup> [34]	0.34 [54]	2.3 [23]	10 <sup>-11</sup> [35]
BP		0.30–2.0 [39]	4.50×10 <sup>4</sup> [40]	1.0 [29]	2.8 [55]	10 <sup>-13</sup> [44]
MoTe <sub>2</sub>		1.1 [56]	1.78×10 <sup>2</sup> [52]	0.90 [57]	3.0 [56]	/
PtSe <sub>2</sub>		0.21–1.2 [49]	2.10×10 <sup>2</sup> [58]	0.72 [59]	2.4 [59]	/
PdSe <sub>2</sub>		0.03–1.4 [50]	2.16×10 <sup>2</sup> [60]	0.77 [60]	2.0 [61]	10 <sup>-15</sup> [53]

example, three main approaches have been previously utilized for developing 2D-material heterogeneous OEICs, namely mechanical exfoliation from graphite [23], CVD growth by using a hydrocarbon gas on a nickel (Ni) or copper (Cu) substrate [67], and epitaxial growth on a silicon carbide substrate [68]. As for the mechanical exfoliation method, it is not suitable for large-scale OEICs production, although it has great potential to provide ultra-high-quality graphene crystals for scientific research. While the CVD and epitaxial growth methods are suitable for mass production. Normally, the CVD method requires some processes to eliminate the catalyst particles (e.g., Ni or Cu) and transfer graphene to other dielectric substrates for developing optoelectronic devices. The graphene epitaxial growth on silicon carbide is known as an ideal material for high-end electronics that might surpass silicon in terms of speed, size, and power consumption, but still suffers from a moderate production rate. As for other 2D materials, numerous excellent papers have been published to review 2D-material preparation for readers' reference [63,66]. To concentrate on the scope of the review, we do not go into details herein.

Due to the planar nature, 2D materials are intrinsically compatible with the fabrication process of OEICs. After developing photonic integrated circuits, 2D materials could be transferred [69,70] or directly grown [71] on the surface of optical waveguides. Different from mechanically exfoliating 2D materials [69], the precise alignment between 2D-material sheets and photonic devices is not required for CVD-growth 2D materials [70], while patterning processes of 2D materials by using lithography facilities are typically necessary to accurately control light-matter interaction in 2D-material hybrid optical waveguides. It is worthwhile to note that researchers also developed a hybrid 2D-material photonic waveguide with bound states in the continuum [72], which transfers nanostructure fabrication from 2D materials to photonic devices, probably avoiding the potential damage to 2D materials during 2D-material patterning processes.

### Light-matter interaction in 2D-material hybrid optical waveguides

Due to the weak light-matter interaction in 2D materials, namely graphene's  $\sim 2.3\%$  absorption to the vertically incident light, several approaches including in-plane evanescent-field light coupling devices [73,74], nanoribbon devices [75], and vertical cavity devices [76], have been explored to overcome the limitation. Among them, the combination of 2D materials and optical waveguides, especially silicon photonic waveguides, is known as a platform of choice for building next-generation optoelectronic devices. On the one hand, the aforementioned 2D materials exhibit unprecedented IR optoelectronic properties in terms of carrier mobility, spectral region, and electrical tunability of Fermi levels, which are expected to break through the fundamental bottlenecks of previous optoelectronic materials. On the other hand, since it was proposed in 1987 [77], silicon photonics provides a revolutionized improvement for integrated optics, making the development of photonic ICs fully compatible not only with microelectronic ICs but also with micro-electro-mechanical systems (MEMS). Consequently, 2D-material heterogeneous optical integration is expected to bring us innovative OEICs with extraordinarily high performances and low costs. In this section, we focus on the previous exploration of the light-matter interaction and the development of passive waveguide devices based on the 2D-material hybrid platforms.

The limitation of the moderate absorption of atomic-layer thick 2D materials to normally incident light could be overcome by using optical waveguide devices. By integrating 2D materials on the surfaces of optical waveguides, the propagating light in the hybrid waveguides can be absorbed by the top-cladding 2D materials through the evanescent-field light coupling configuration. In 2012, Li *et al.* [78] experimentally demonstrated that the graphene-induced absorption coefficient could be as high as  $0.2 \text{ dB}/\mu\text{m}$  when graphene was located directly on the surface of a silicon waveguide which was measured by using an on-chip Mach-Zehnder interferometer (MZI) device [78], as shown in Figure 2A. Later, the study of developing 2D-material hybrid optical devices was widely extended to silicon nitride [79–81], polymer [82], zinc oxide [83], and chalcogenide glass [84] waveguides with graphene [85] or TMDs [86,87] sheets integrated on top, as shown in Figure 2B. Furthermore, the in-plane interaction between 2D materials and on-chip propagating light can be enhanced by utilizing chip-integrated micro/nanocavities [80,88–92] or light nanoconfinement structures [93]. For example, in 2015, Wang *et al.* [80] experimentally studied graphene-integrated silicon nitride microring resonators, showing that there should be a trade-off between the increased graphene length and sacrificed quality ( $Q$ ) factor of the microring resonators for the development of cavity-enhanced

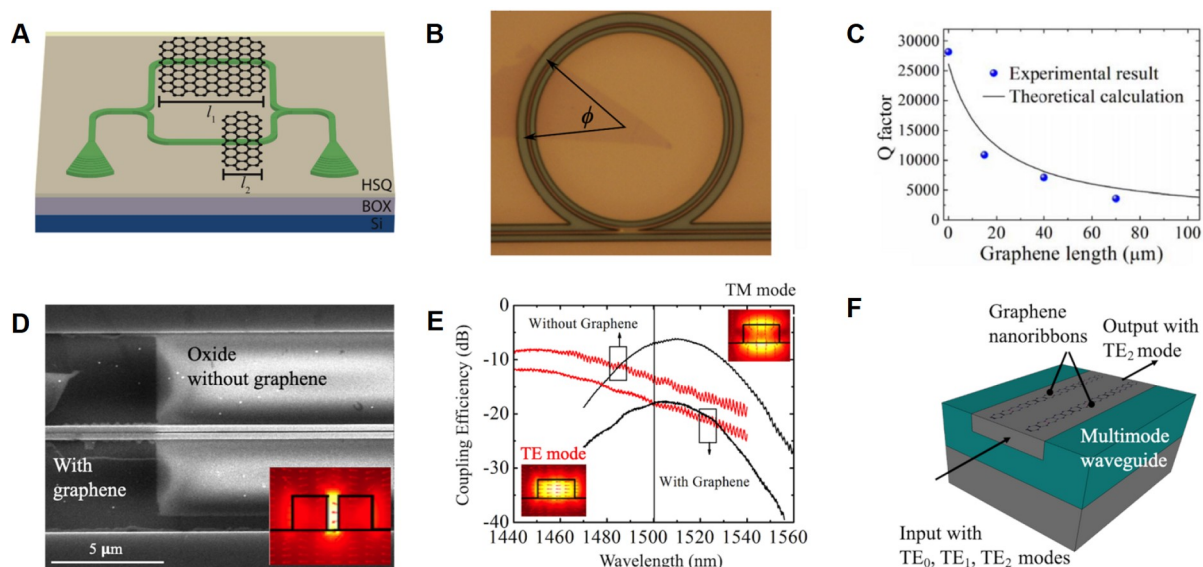


**Figure 2** Studies of the optical absorption and the development of the passive devices based on 2D-material hybrid waveguides. (A) Schematic of the graphene-on-silicon optical device for measuring the graphene-introduced optical absorption coefficient [78]. (B) Optical image of a device with the ring covered by a monolayer MoS<sub>2</sub> over a circumference corresponding to  $\Phi=\pi/4$  [87]. (C) Measured  $Q$ -factor of the graphene-on-silicon nitride microring resonator as a function of the graphene length [80]. (D) Scanning electron microscope (SEM) image of the graphene-on-silicon slot waveguide [93]. The inset is the electric-field distribution of the silicon slot waveguide. (E) Measurement of the polarization-dependent transmission of the graphene-on-silicon waveguide [69] coupled by using the polarization-insensitive focusing subwavelength gratings [112]. The insets are the electric-field distributions of the TE<sub>0</sub> and TM<sub>0</sub>-mode waveguides. (F) Schematic of the on-chip TE<sub>2</sub> mode filter based on the graphene-on-silicon multimode waveguide [109].

optoelectronic devices, as shown in Figure 2C. In the same year, Cheng *et al.* [93] demonstrated that, with the strong light confinement, the silicon slot waveguide could improve graphene’s absorption of the propagating light by a factor of about two compared with that of the conventional stripe waveguide, as shown in Figure 2D. In short, the waveguide-enhanced optical absorption brings us great opportunities to develop on-chip 2D-material hybrid photonic devices.

Besides the linear optical absorption, researchers also extensively explored nonlinear optical absorption characteristics, namely saturable absorption [73,94–98], spectral hole burning [99], and optically induced transparency effects [100], based on 2D-material hybrid optical waveguide devices. Compared with the device configurations with the normal light incidence, the waveguide-integrated platforms provide larger flexibility to tailor the characteristics of the graphene’s nonlinearity through adjusting in-plane interaction lengths. Moreover, photon-generated free carriers and heat in graphene play a significant role in the manipulation of the propagating light in optical waveguides, enabling all-optical modulation applications [73,100–106]. As early as 2013, Cheng *et al.* [73] demonstrated the all-optical modulation based on a graphene-on-silicon waveguide. Due to the limited free-carrier lifetime in silicon devices, the all-optical modulation speed was just around the 100-kHz frequency. Later, in 2020, Ono *et al.* [103] demonstrated ultrafast all-optical switching with a switching time of only 260 fs in a plasmonic-waveguide-integrated suspended graphene device based on the nonlinear saturable absorption effect. The all-optical modulation/switching paves the way towards on-chip photonic signal processing with low energy consumption. More nonlinear optical effects, such as nonlinear frequency conversion, reflecting nonlinear interaction between propagating light and on-chip 2D materials are discussed in Section “On-chip 2D-material lasers”.

Based on 2D-material hybrid waveguides, various on-chip functional devices, such as polarizers [107,108], mode filters [109], and grating couplers [110], have been developed by exploring the spatial overlap between electric-field distributions in the waveguides and graphene sheets. For example, in 2013, Cheng *et al.* [107] demonstrated that optical absorption coefficients of graphene-on-silicon waveguides depended on the propagating light polarization, namely fundamental transverse-electric ( $TE_0$ ) and transverse-magnetic ( $TM_0$ ) modes, due to the different modal energy distributions around the graphene sheet, as shown in Figure 2E. In 2018, Xing *et al.* [111] designed an on-chip polarizer based on a graphene-on-silicon nanowire. They obtained a polarization extinction ratio of 20.1 dB and a low optical loss of 0.68 dB for the  $TE_0$  mode via a 150- $\mu\text{m}$ -long nanowire. Later, by integrating graphene nanoribbons on multimode silicon waveguides, the same group further studied the on-chip graphene-based  $TE_1$ -mode-pass and  $TE_2$ -mode-pass filters which could be used for mode-division multiplexing applications [109], as shown in Figure 2F. In summary, the studies of the in-plane interaction between propagating light in optical waveguides and waveguide-integrated 2D-material sheets lay a foundation for exploring advanced OEICs.

### On-chip 2D-material lasers

Due to the indirect bandgap, silicon is not a natural creator of light, while 2D materials have several advantages for the development of waveguide-integrated lasers. First, some 2D materials, such as TMDs, have strong photoluminescence characteristics because their energy band structures can transform from indirect to direct features when the materials are reduced to monolayer thicknesses. As a result, the 2D materials could be used as gain media for lasing development [113]. Second, the saturable absorption properties of 2D materials make them suitable for developing on-chip Q-switching or mode-switching lasers [114,115]. Moreover, with the enhanced light-matter interaction on a chip, 2D-material lasers could have low thresholds and large waveguide-coupled powers [116]. Generally, on-chip 2D-material lasers may be divided into two types: lasers based on electron transitions and lasers based on optical nonlinearities. Compared with 2D-material modulators and photodetectors, few studies of on-chip 2D-material lasers have been reported. Consequently, in this section, we discuss the advances of the two types of on-chip 2D-material lasers with the spectral range covering from visible light to IR wavelengths.

As for the development of on-chip 2D-material lasers based on electron transitions, monolayer TMDs were selected as the main gain media integrated on high  $Q$ -factor micro-resonators. After pumping by high-power lasers, the devices could emit coherent light with spectra covering from visible light to IR wavelengths. In 2015, Wu *et al.* [113] demonstrated the on-chip TMD laser at the wavelength of 740 nm by integrating a monolayer  $\text{WSe}_2$  sheet on a photonic crystal (PhC) cavity. It is worthwhile to note that the laser has to be operated at cryogenic temperatures. When the temperature increased to about 250 K, the laser diminished into the background spontaneous emission. In the same year, Ye *et al.* [117] demonstrated the on-chip  $\text{WS}_2$  lasers also at cryogenic temperatures by integrating a monolayer  $\text{WS}_2$  on a microdisk resonator. To develop on-chip 2D-material lasers at room temperature, cavities with higher  $Q$ -factors are necessary. In 2015, Salehzadeh *et al.* [118] studied the on-chip  $\text{MoS}_2$  laser at room temperature. The laser was fabricated based on a  $\text{SiO}_2$  microdisk resonator with a  $Q$  factor of 3300. The laser's center wavelength and threshold were measured as 664 nm and 30  $\mu\text{W}$ , as shown in Figure 3A. In 2017, Li *et al.* [119] further extended the

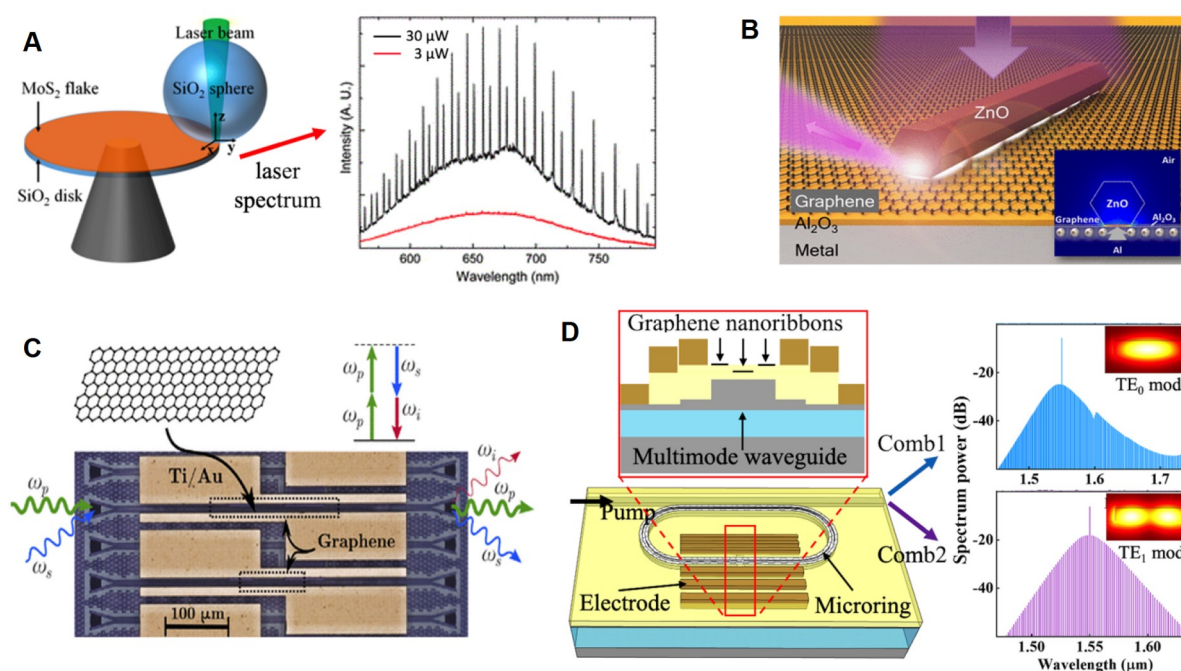


**Figure 3** Studies of the on-chip 2D-material lasers. (A) Schematic of the MoS<sub>2</sub> laser based on the SiO<sub>2</sub> microdisk cavity [118]. (B) Schematic of the graphene surface plasmon polariton nanolaser [116]. (C) Optical image of the graphene-on-silicon nitride waveguide for the four-wave mixing generation [120]. (D) Schematic of the graphene-enabled dual-mode Kerr frequency comb generation [115].

wavelength of room-temperature on-chip TMDs lasers to IR wavelengths based on MoTe<sub>2</sub>. Besides TMDs, graphene is also studied for developing on-chip lasers. In 2019, Li *et al.* [116] demonstrated a graphene plasmonic nanolaser based on a Fabry-Perot (F-P) cavity, as shown in Figure 3B. In this work, graphene enhances the electron density at the metal surface, resulting in a blue-shift of the metal plasmon frequency. Later, Li *et al.* [114] demonstrated that the threshold of the graphene laser could be modulated by external currents. In Table 2, we summarized the experimental results of the on-chip 2D-material lasers based on electron transitions.

Besides, on-chip nonlinear lasers based on 2D materials, especially graphene and graphene oxide, have attracted great attention in the past decade. Due to the giant Kerr nonlinearity of graphene and graphene oxide [121–124], the hybrid waveguides exhibit stronger four-wave mixing than those of the waveguide without graphene [125–127]. In 2012, Gu *et al.* [128] demonstrated that a monolayer graphene sheet could improve the conversion efficiency of the four-wave mixing in a silicon PhC cavity by a factor of around 30 dB,

**Table 2** Comparison of the demonstrated on-chip 2D-material lasers

Material	Cavity type	Gain medium	Q factor	Operation temperature (K)	Lasing threshold	Lasing wavelength (nm)	Ref.
WSe <sub>2</sub>	PhC waveguide	WSe <sub>2</sub>	2465	80–160	27 (nW)	740	[113]
WS <sub>2</sub>	Microdisk resonator	WS <sub>2</sub>	2604	10	5 (mW/cm <sup>2</sup> )	612	[117]
MoS <sub>2</sub>	Microdisk resonator	MoS <sub>2</sub>	3300	300	30 (μW)	664	[118]
MoTe <sub>2</sub>	PhC waveguide	MoTe <sub>2</sub>	5603	300	97 (μW)	1132	[119]
Graphene	F-P cavity	ZnO	/	77	77 (μW)	373	[114]
Graphene	F-P cavity	ZnO	/	77–300	18.5 (mW/cm <sup>2</sup> )	373	[116]

opening an avenue to develop highly nonlinear devices based on 2D-material hybrid waveguides. In 2015, Ji *et al.* [129] demonstrated the graphene-enhanced parametric frequency conversion based on a silicon microring resonator. In this work, the maximum enhancement factor of 6.8 dB in the conversion efficiency was observed experimentally. To further increase the frequency conversion bandwidth, Yang *et al.* [130] optimized the interaction length between propagating light and graphene, and demonstrated that the four-wave mixing conversion bandwidth could be increased to 35 nm. Later, Alexander *et al.* [120] experimentally showed that the four-wave mixing conversion efficiency strongly depended on the Fermi level of the graphene. The optical microscope image of the devices is presented in Figure 3C. In 2018, Yao *et al.* [131] demonstrated a tunable graphene-on-silicon-nitride-waveguide-integrated Kerr frequency comb. The free spectral range of the comb could be tuned within 2.36–7.17 THz by an external electric field that was applied to the graphene sheets. The authors explained that the phenomenon is attributed to the variation of the graphene's Fermi level that results in the dispersion change of the hybrid micro-resonator. In 2022, Chen *et al.* [115] theoretically studied a dual-mode Kerr frequency comb based on a graphene-on-silicon microring resonator, as shown in Figure 3D. By carefully designing the graphene nanoribbons on the multi-mode silicon waveguide,  $TE_0$ -mode and  $TE_1$ -mode Kerr frequency combs could be selectively activated via modulating the Fermi level of the graphene nanoribbons, which is expected to provide a key technique for developing advanced multiplexing light sources for optical communications and interconnects. In brief, the development of on-chip 2D-material lasers is still in its infancy nowadays in terms of energy conversion efficiency and spectral bandwidth, especially for IR wavelengths, although the above great efforts have been made in the past decade.

### On-chip 2D-material electro-optical modulators

Due to the low carrier densities of 2D materials, their Fermi levels could be easily tuned by using external electric fields, seriously influencing the intensity and phase of the propagating light in optical waveguides after integrating 2D materials on the surface of devices. Therefore, it provides the promising potential for developing on-chip electro-optical modulators for wide applications in optical communications, interconnects, and switching. Compared with previous on-chip electro-optical modulation techniques with the capability of modulating light at frequencies of up to 100 GHz, such as silicon or III-V modulators based on the free-carrier-induced RI and absorption variations [132,133], organic polymer or  $LiNbO_3$  modulators based on the Pockels effect [134,135], and semiconductor modulators based on the quantum-confined Stark effect [136], 2D-material modulators may have the merits of higher modulation speeds due to the high carrier mobilities, low power consumptions resulting from the low carrier densities, small device footprints due to the strong on-chip light-matter interaction, environment-friendly material preparation process, as well as potentially complementary metal-oxide-semiconductor (CMOS)-compatible device fabrication. Moreover, for efficiently modulating the carrier densities of 2D materials, one crucial technical issue that needs to be considered is to properly engineer the interfaces between 2D materials and substrates or metal contacts. For the underneath substrates, the tunability of Fermi levels might be weakened due to the Fermi level pinning (FLP) effect caused by 2D materials-semiconductor interface states [137]. An ultraclean transfer process [138] or a passivation layer, such as an hBn [139] or atomic-layer-deposition  $Al_2O_3$  [140] layer, is usually

required before transferring 2D materials on waveguides. Besides, large metal contact resistance may also reduce the modulation efficiency of 2D materials-based devices. Several approaches have been demonstrated to reduce the 2D materials' contact resistance including edge contact [141], using semimetals to achieve Ohm contact [142], or inducing traps at the contact area. Since most experimental results of the waveguide-integrated 2D-material electro-optical modulators are developed based on graphene, in this section, we only focus on the study of waveguide-integrated graphene electro-optical modulators.

The intensity modulation is the main approach to developing graphene electro-optical modulators, which were studied by integrating a graphene FET on a silicon rib waveguide in 2011 [31]. In such modulators, the graphene absorption to propagating light in optical waveguides can be electrically modulated by alternating the Fermi level below and beyond the half photon energy of the propagating light. After the first modulator demonstration, the same group reported another dual-layer graphene modulator with GHz frequencies on the silicon waveguide [143], as shown in Figure 4A. Compared with the first graphene modulator in their previous study [31], the improved device could break the limitations of the modulation speed caused by the carrier injection in the silicon waveguide, and further improved the modulation depth by using the dual-layer graphene sheets. Since then, various studies of on-chip graphene intensity modulators [144–151] have been widely demonstrated by improving graphene absorption strength to the propagating light and device operation bandwidth. For example, microring resonators are employed to integrate with graphene for developing modulators [140,152–154], as shown in Figure 4B. Through tuning the round-trip attenuation, it is possible to change the transmission of the graphene hybrid microring at the resonant wavelengths [153]. Although the microring configuration greatly reduces the footprints of the modulator, it usually suffers from

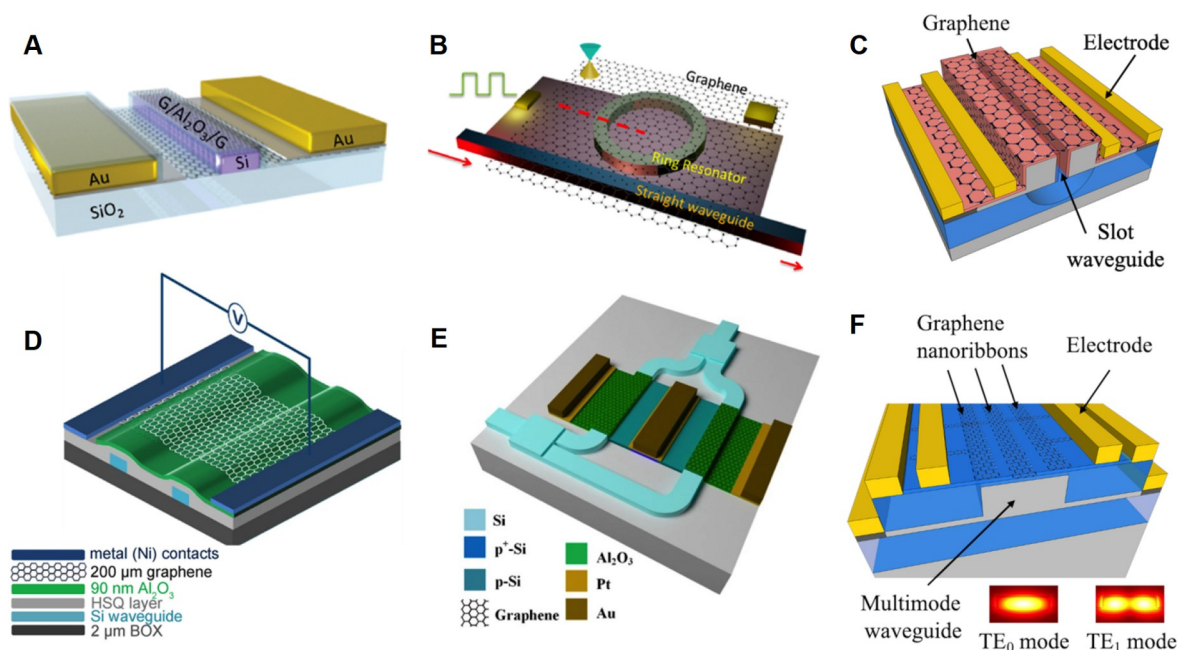


**Figure 4** Studies of the waveguide-integrated graphene electro-optical modulators. (A) Schematic of the dual-layer graphene intensity modulator [143]. (B) Schematic of the graphene-on-silicon microring intensity modulator [154]. (C) Schematic of the graphene-on-silicon slot waveguide intensity modulator [155]. (D) Schematic of the graphene phase modulator based on the MZI structure [160]. (E) Schematic of the graphene modulator based on the MZI structure. The intensity and phase modulation modes can be switched by using different driving voltages [161]. (F) Schematic of the dual-mode modulator based on the graphene-nanoribbon-on-silicon waveguide [163].

limited operation wavelengths. Moreover, optical waveguides with light confinement at the nanoscale, such as silicon slot waveguides [155], and plasmonic waveguides [156–158], have been proposed for studying compact graphene modulators. For instance, in 2016, Phatak *et al.* [155] proposed and theoretically studied graphene-on-silicon slot waveguide modulators as shown in Figure 4C. With the merits of the nanostructured waveguide and suspended graphene sheet, it is much easier to tune the graphene's Fermi level compared with the graphene-integrated  $TM_0$ -mode waveguide, reducing the device length by a factor of two with the same modulation depth.

The research progress of graphene phase modulators is still far behind that of the graphene intensity modulators. For graphene phase modulators, the Fermi level of graphene is tuned beyond half of the photon energy of propagating light, which mainly changes the real part of the relative permittivity of graphene, modulating the phase of propagating light in optical waveguides. Nowadays, several groups experimentally demonstrated waveguide-integrated graphene phase modulators [159–162]. As shown in Figures 4D and E, the on-chip MZI devices are commonly employed. It is worthwhile to note that the phase variations induced by the top-layer graphene sheets are usually weak, while it is easy to break down the graphene capacitance devices under extremely high bias voltages (BVs). Consequently, phase changes of the propagating light in optical waveguides are typically weak in graphene phase modulators, resulting in large device footprints. It is important to enhance the light-matter interaction by using high-quality and ultra-thin isolated layers between graphene sheets and waveguides, as well as nanostructured waveguides, such as slot waveguides [155] and PhC waveguides [162]. Moreover, it is promising to develop graphene phase modulators with diverse modulation formats and multiplexing techniques. For example, in 2020, the researchers proposed and theoretically studied binary phase-shift keying (BPSK) graphene modulators with the  $TE_0$ -mode and  $TE_1$ -mode operation based on the dual-layer graphene nanoribbons integrated waveguide microring [163] and MZI [164] configurations, as shown in Figure 4F. Besides Fermi level tuning, graphene could also be worked as an excellent thermal heater to change the RIs of silicon waveguides for developing thermo-optical modulators [165,166]. In Table 3, we summarized the performance of the experimentally demonstrated waveguide-integrated graphene electro-optical modulators.

### On-chip 2D-material photodetectors

Various 2D-material photodetectors have been extensively studied [167,168] since graphene was reported in 2004 [23]. Integrating 2D materials on optical waveguides not only helps improve the photodetection responsivity of 2D materials compared with the device configurations with normally incident light but also brings us significant advances in the development of on-chip optoelectronic systems. According to previous studies, several photodetection mechanisms, such as the photovoltaic (PV) effect [169], photothermoelectric (PTE) effect [170], and bolometric (BOL) effect [171], have been proposed to explain photo-electron conversion processes in waveguide-integrated 2D-material photodetectors. As for the PV effect, photocurrents generate from electron-hole pairs driven by built-in or applied electric fields. On the other hand, PTE and BOL currents are both driven by the thermal mechanism. The difference between the PTE and BOL effects lies in that the PTE currents are typically induced by the ultrafast heating of carriers in 2D materials, while the BOL currents are normally induced by the transport conductance change of 2D materials due to

**Table 3** Summary of the demonstrated 2D-material electro-optical modulators

Material	Operation wavelength ( $\mu\text{m}$ )	3-dB bandwidth (GHz)	Modulation type	Device structure	Modulation depth	Device footprint ( $\text{mm}^2$ )	Ref.
Graphene	1.35–1.60	1	Intensity	SOI waveguide	0.1 (dB/ $\mu\text{m}$ )	$2.5 \times 10^{-5}$	[31]
Dual-layer graphene	1.55	1	Intensity	SOI waveguide	0.16 (dB/ $\mu\text{m}$ )	$10^{-5}$	[143]
Dual-layer graphene	1.54–1.64	35	Intensity	SOI waveguide	0.067 (dB/ $\mu\text{m}$ )	$1.8 \times 10^{-5}$	[144]
Graphene	1.55	5.9	Intensity	SOI waveguide	0.05 (dB/ $\mu\text{m}$ )	$5 \times 10^{-4}$	[145]
Graphene	1.55	10	Intensity	SOI waveguide	0.055 (dB/ $\mu\text{m}$ )	/	[146]
Dual-layer graphene	1.55	0.67	Intensity	SOI waveguide	0.053 (dB/ $\mu\text{m}$ )	$10^{-3}$	[147]
Dual-layer graphene	1.55	2.5	Intensity	SOI waveguide	4.437 (dB)	$10^{-4}$	[148]
Graphene	429–2000	5	Intensity	SOI waveguide	10 (dB)	1	[149]
Dual-layer graphene	1.55	12	Intensity	PhC waveguide	0.055 (dB/ $\mu\text{m}$ )	$10^{-5}$	[150]
Graphene	1.55	/	Phase	PhC waveguide	8 (dB)	/	[165]
Dual-layer graphene	1.55	29	Intensity	SOI waveguide	0.025 (dB/ $\mu\text{m}$ )	$10^{-2}$	[151]
Graphene	1.55	30	Intensity	$\text{Si}_3\text{N}_4$ microring	28 (dB)	/	[140]
Dual-layer graphene	1.59	14.7	Intensity	$\text{Si}_3\text{N}_4$ microring	7 (dB)	$10^{-5}$	[152]
Graphene	1.55	/	Intensity	SOI microring	12.5 (dB)	$10^{-2}$	[153]
Graphene	1.55	/	Intensity	SOI microring	2.3 (dB)	$10^{-5}$	[154]
Graphene	1.55	774	Phase	SOI microring	7 (dB)	$10^{-5}$	[166]
Graphene	1.5	/	Intensity	Plasmonic waveguide	0.03 (dB/ $\mu\text{m}$ )	$10^{-5}$	[156]
Dual-layer graphene	1.55	/	Intensity	Slot waveguide	0.13 (dB/ $\mu\text{m}$ )	$10^{-5}$	[157]
Dual-layer graphene	1.53–1.57	/	Intensity	Slot waveguide	0.036 (dB/ $\mu\text{m}$ )	$10^{-4}$	[158]
Graphene	1.55	5	Phase	SOI MZI	35 (dB)	$10^{-1}$	[159]
Dual-layer graphene	1.53–1.57	/	Phase	SOI MZI	15 (dB)	$10^{-1}$	[160]
Graphene	1.55	/	Intensity & Phase	SOI MZI	25 (dB)	$10^{-1}$	[161]
Graphene	1.55	67	Phase	PhC MZI	/	$10^{-3}$	[162]

temperature variations associated with incident photons. Due to the different photodetection mechanisms, waveguide-integrated 2D-material photodetectors exhibit distinct performances in terms of responsivity, detectivity, dark current, operation wavelength, and bandwidth. In this section, we discuss the experimental results of waveguide-integrated 2D-material photodetectors.

Waveguide-integrated 2D-material photodetectors were reported based on graphene in 2013 [69,172,173], in which mechanically exfoliated graphene sheets were used as photosensitive materials. In the telecommunication band, a maximum responsivity of 0.1 A/W with an operating bandwidth of 20 GHz was demonstrated [172] based on the PV effect. Apart from forming the built-in electric field in the graphene channel which overlapped with the evanescent field of the propagating light, researchers also utilized a graphene/silicon Schottky diode by directly integrating a graphene sheet on a silicon suspended membrane waveguide [174] to detect photocurrents [69] (Figure 5A). With the improvement of graphene synthesis techniques based on the CVD-growth process [175,176], researchers demonstrated numerous waveguide-integrated CVD-growth graphene photodetectors [177–181] with a maximum operation bandwidth of 41 GHz [177], providing the possibility of fabricating scalable systems on a chip. To further enhance the graphene's optical absorption, various waveguides have been utilized to develop photodetectors, such as slot waveguides [70,182], ultra-thin waveguides [183], PhC waveguides [184,185], and plasmonic waveguides [186–188]. For example, Wang *et al.* [70] demonstrated a graphene-on-silicon slot waveguide photodetector in 2016 which is based on the PTE effect, as shown in Figure 5B. With the enhanced optical absorption caused by the nanoconfinement of light in the slot waveguide, a maximum responsivity of 0.273 A/W was obtained with only a 20- $\mu\text{m}$ -long active region. Besides the SOI platform, researchers explored other

integrated platforms for developing on-chip graphene photodetectors, such as silicon dioxide [189] and silicon nitride [180,190,191]. For instance, in 2015, Wang *et al.* [192] demonstrated a graphene-on-silicon nitride waveguide photodetector based on the BOL effect. A microring resonator with a length-optimized graphene sheet was developed to achieve a responsivity of 1.31 mA/W at 1.55  $\mu\text{m}$  wavelengths. It is worthwhile to note that graphene integration provides great potential for developing low-cost optoelectronic devices on silicon nitride waveguides, which exhibit ultra-low optical losses but lack the capability of modulation and photodetection due to the isolator nature. After years of device development, on-chip graphene photodetectors have been developed to construct on-chip optical coherent receivers with the receptions of 90 Gbit/s BPSK, 200 Gbit/s quadrature phase-shift keying, and 240 Gbit/s 16 quadrature amplitude modulation signals [193] (Figure 5C). Although the speed of graphene photodetectors is still slower than germanium (up to 265 GHz) [194] and InP diodes (up to 170 GHz) [195] at the telecommunication band, the merits of ultrahigh carrier mobility and moderate requirements of the lattice match for heterostructure integration make graphene as a promising candidate to explore high-performance on-chip photodetection.

Besides the above on-chip graphene photodetectors at 1.55- $\mu\text{m}$  wavelengths, waveguide-integrated 2D-material photodetectors have been explored with longer wavelengths and multiply materials. For example, Guo *et al.* [187] demonstrated a waveguide-integrated graphene photodetector at 2- $\mu\text{m}$  wavelengths (Figure 5D). By integrating a graphene sheet on a plasmonic waveguide, the authors demonstrated a responsivity of 70 mA/W and an operating bandwidth of 20 GHz. On the other hand, although graphene photodetectors have the merits of broad spectral operation band and high speed, the gapless band structure usually results in large dark currents. To overcome this problem, other 2D materials with bandgap structures, such as BP, PtSe<sub>2</sub>, and

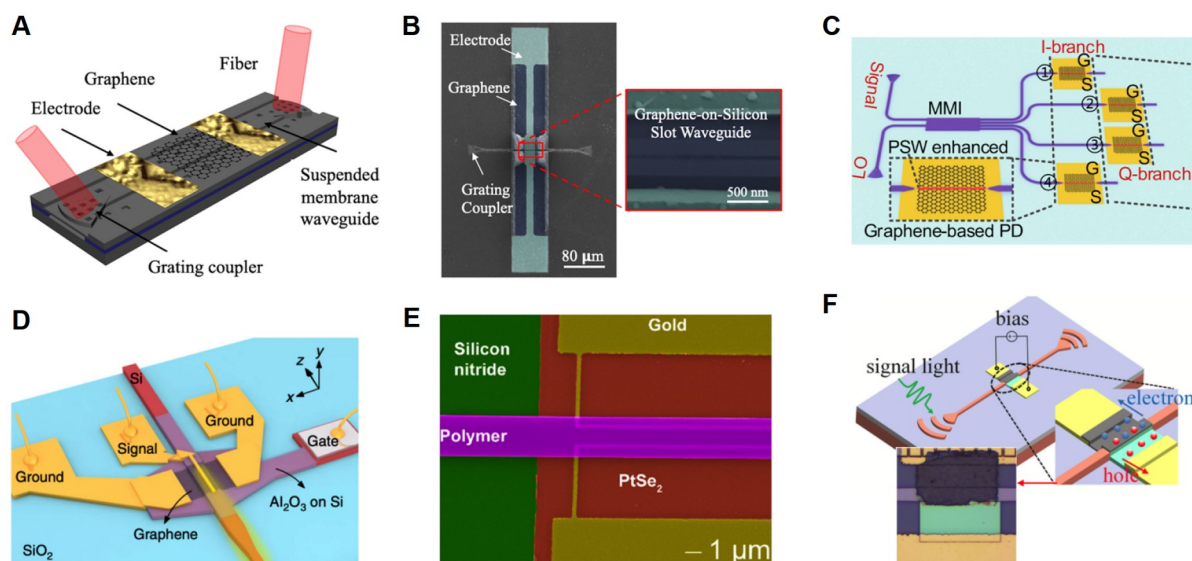


**Figure 5** Study of the waveguide-integrated 2D-material photodetectors. (A) Schematic of the graphene-on-silicon heterostructure photodetector [69]. (B) False-color SEM image of the graphene-on-silicon slot waveguide photodetector [70]. (C) Schematic of the on-chip graphene optical coherent receiver based on the plasmonic waveguide [193]. (D) Schematic of the graphene-on-silicon photodetector at 2- $\mu\text{m}$  wavelengths [187]. (E) False-color SEM image of the PtSe<sub>2</sub> photodetector with the bound-states-in-continuum waveguide integration [200]. (F) Schematic and image of the Ti<sub>3</sub>C<sub>2</sub>T<sub>x</sub>/p-Si waveguide-integrated photodetector [201]. The inset is the false-color optical image of the photodetector.

MXene, have been investigated to develop on-chip photodetectors. Nowadays, silicon-waveguide-integrated BP photodetectors at 1.55- $\mu\text{m}$  wavelengths with the GHz-frequency operating bandwidth at the telecommunication band [196,197] and high responsivities at mid-IR wavelengths [198,199] have been demonstrated. While Wang *et al.* [200] demonstrated a PtSe<sub>2</sub> photodetector with bound-states-in-continuum waveguide integration on a silicon nitride wafer (Figure 5F), with a responsivity of 12 mA/W and an operating bandwidth of 35 GHz at 1.55- $\mu\text{m}$  wavelengths. Compared with the BP photodetectors, the on-chip PtSe<sub>2</sub> photodetector may have better environmental stability due to the material's superiority in oxidation resistance. Furthermore, Yang *et al.* [201] demonstrated a p-doped silicon waveguide-integrated Ti<sub>3</sub>C<sub>2</sub>T<sub>x</sub> photodetector with a responsivity of 40  $\mu\text{A/W}$  in the telecommunication band, shown in Figure 5F. By using a vacuum annealing method, the barrier of the Ti<sub>3</sub>C<sub>2</sub>T<sub>x</sub>/p-Si Schottky photodetector could be adjusted from 0.64 to 0.72 eV, leading to a 215-nm blue-shift of working wavelength. Besides, couples of vertical van der Waals heterostructures, namely graphene/MoS<sub>2</sub> [202], MoTe<sub>2</sub>/graphene [203], graphene/boron nitride (BN) [204], and graphene/multilayer BN/graphene/MoS<sub>2</sub> [205] heterostructures, have been also demonstrated to attain a large responsivity, high operation bandwidth, and minimized dark current with the integration of waveguide devices. In Table 4, we summarized the performance of the experimentally demonstrated 2D-material photodetectors.

## Summary and prospect

In this review, we summarize the optoelectronic properties of 2D materials and their applications in heterogeneous optoelectronic integration. Specifically, we first compare five types of the currently discovered 2D materials that can be employed to develop IR optoelectronic devices and introduce the fabrication of 2D-material heterogeneous OEICs. We then summarize leading-edge advances in 2D-material waveguide-integrated devices including the on-chip functional passive devices, lasers, electro-optical modulators, and photodetectors. Although the aforementioned optoelectronic devices have experienced prosperous development in the past decade, integrated optoelectronics with 2D materials is still a sunrise direction for research and development. There is plenty of room for the improvement of 2D-material heterogeneous OEICs in the future, shown in Figure 6.

(1) It will be interesting to tailor the optoelectronic properties of 2D materials by engineering electronic bands or exploring heterostructures on a chip. On the one hand, electronic bands of 2D materials can be optimized by patterning 2D materials to nanostructures [208], or selecting suitable electrostatic gating or doping methods [209]. On the other hand, by taking the advantage of 2D-material heterostructures, namely lateral 2D monolayer heterostructure and vertical 2D stacking multilayer heterostructure, it can not only elaborately engineer the energy bandgaps of van der Waals 2D material [210] to improve the photocurrent on/off ratios in 2D-material transistors but also significantly modify the energy band diagram of 2D materials, namely through controlling twisted magic angles [211] between adjacent 2D-material layers. Moreover, mixture heterostructures consisting of 2D materials with 0D/1D materials, namely lead sulphide-cadmium sulphide quantum dots [212] and mercury telluride quantum dots [213], are promising approaches to increase photon capture capabilities in materials for improving their responsivities and extending spectral bandwidths [214,215]. By integrating the band-engineered 2D materials or 2D-material heterostructures on optical

**Table 4** Summary of the demonstrated 2D-material photodetectors

2D material	Operation wavelength (μm)	Operation bandwidth (GHz)	Detection mechanism	Device structure	Detection responsivity	Dark current (nA)	Ref.
Graphene	1.55	20	PV	SOI waveguide	0.108 (A/W)	/	[172]
Graphene	1.55	42	PV	SOI waveguide	0.016 (A/W)	/	[177]
Graphene	1.55	/	PV	SOI waveguide	0.37 (A/W)	20 (BV: 1 V)	[178]
Graphene	1.55	18	PV	SOI waveguide	0.05 (A/W)	/	[173]
Graphene	1.55	/	PV	Glass waveguide	0.72 (A/W)	/	[189]
Graphene	0.53	/	PV	Si <sub>3</sub> N <sub>4</sub> waveguide	0.44 (A/W)	/	[202]
Graphene	1.55	17	PV	SOI waveguide	0.025 (A/W)	/	[183]
Graphene	1.55	5	PV	SOI waveguide	0.0008 (A/W)	/	[184]
Graphene	1.55/2.75	/	PV	SOI waveguide	0.0001/0.13 (A/W)	10 (BV: -1.5 V)	[69]
Graphene	1.55	38	PV	Si <sub>3</sub> N <sub>4</sub> waveguide	0.013 (A/W)	10 <sup>5</sup> (BV: 0.1 V)	[206]
Graphene	1.55	70	PV	Plasmonic waveguide	0.1 (A/W)	/	[186]
Graphene	1.55	30	PV	SOI waveguide	0.015 (A/W)	/	[179]
Graphene	1.55	28	PV	Si <sub>3</sub> N <sub>4</sub> waveguide	0.24 (A/W)	13 (BV: 10 V)	[205]
PtSe <sub>2</sub>	1.55	35	PV	Si <sub>3</sub> N <sub>4</sub> waveguide	0.012 (A/W)	317 (BV: 8 V)	[200]
MoTe <sub>2</sub> /graphene	1.55	50	PV	SOI waveguide	0.2 (A/W)	0 (BV: 0 V)	[203]
BP	1.55	3	PV	SOI waveguide	0.657 (A/W)	220 (BV: -0.4 V)	[196]
BP	1.55	0.15	PV	SOI waveguide	10 (A/W)	/	[197]
BP	3.68-4.03	/	PV	SOI waveguide	23 (A/W)	100 (BV: 0 V)	[198]
BP	2.0	1.33	PV	SOI waveguide	0.3067 (A/W)	/	[199]
Ti <sub>3</sub> C <sub>2</sub> T <sub>x</sub>	1.55	/	PV	SOI waveguide	4×10 <sup>-5</sup> (A/W)	10 <sup>-4</sup> (BV: 0 V)	[201]
Graphene	1.55	/	PTE	Slot waveguide	0.273 (A/W)	/	[70]
Graphene	1.55	18	PTE	PhC waveguide	0.17 (A/W)	/	[185]
Graphene	1.55	20	PTE	SOI waveguide	0.4 (A/W)	3×10 <sup>6</sup> (BV: -0.3 V)	[187]
Graphene	1.55	70	PTE	SOI waveguide	3.5 (V/W)	0	[170]
Graphene	1.55	67	PTE	Si <sub>3</sub> N <sub>4</sub> waveguide	6 (V/W)	0	[191]
Graphene	1.55	65	PTE	Slot waveguide	0.076 (A/W)	/	[182]
Graphene	1.55	33	PTE	Si <sub>3</sub> N <sub>4</sub> waveguide	2.36 (A/W)	/	[180]
Graphene	1.55	42	PTE	SOI waveguide	0.36 (A/W)	0	[204]
Graphene	1.55	/	PTE	Si <sub>3</sub> N <sub>4</sub> waveguide	0.126 (A/W)	/	[190]
Graphene	1.55	76	BOL	SOI waveguide	0.001 (A/W)	/	[181]
Graphene	1.55	110	BOL	SOI waveguide	0.5 (A/W)	6×10 <sup>6</sup> (BV: 0.6 V)	[188]
Graphene	1.31	/	BOL	Plasmonic waveguide	0.67 (A/W)	2.3×10 <sup>4</sup> (BV: -1 V)	[207]
Graphene	1.55	/	BOL	SOI waveguide	0.11 (A/W)	1.45×10 <sup>6</sup> (BV: 1 V)	[171]

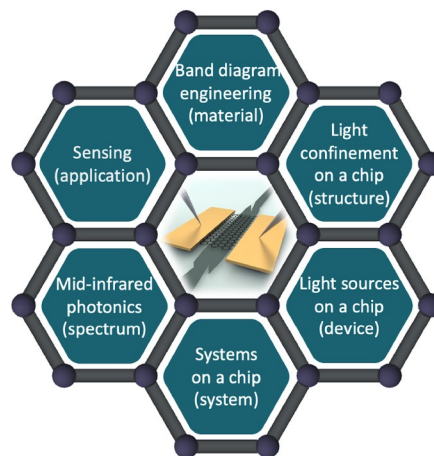


**Figure 6** Potential areas deserving to explore for developing 2D-material heterogeneous OEICs in the future.

waveguides, it is expected to explore novel optoelectronic devices with unprecedented performances.

(2) 2D materials are promising to develop novel waveguide-integrated light sources. For example, strain engineering techniques could be utilized on 2D materials even during material growth [216,217]. Therefore, it may be possible to develop electrically pumped on-chip single-photon light emitters for quantum computing, unconditional quantum cryptography, and quantum communications. Besides, waveguide-integrated light sources based on optical nonlinearity, such as on-chip Kerr frequency combs, may also play an important role in this area, due to giant nonlinear RIs of 2D materials. Moreover, some nonlinear optical effects [218,219] which have been observed in graphene-covered optical fiber devices have not been studied on 2D-material heterogeneous OEICs.

(3) Nanostructured devices are expected to bring more opportunities to improve the performances of OEICs with 2D materials. On the one hand, photonic/plasmonic waveguide devices with excellent capability to confine light at the nanoscale could be studied by using the plasmonic [220] or subwavelength devices [221]. On the other hand, patterned 2D-material nanostructures [222] could also be developed on the surface of waveguide devices for improving the strength and manner of the on-chip light confinement in 2D materials [223,224]. Based on innovative designs of 2D-material-integrated nanostructured photonic devices, it is possible to further minimize optoelectronic devices' footprints as well as improve the operating speeds. Furthermore, since plasmons could be excited at the mid-IR even near-IR spectral region in 2D materials (e.g., graphene) [225,226], it opens an avenue to develop atomic-layer thickness plasmonic integrated circuits with ultracompact footprints and flexible electric-gate tunability for optical interconnects and sensing.

(4) It is necessary to develop complex systems on a chip (SoC) by integrating multiple 2D-material optoelectronic devices with high density and large volumes. Although the single functional devices, such as modulators and photodetectors, have been developed to achieve state-of-the-art performances, on-chip transceivers with advanced modulation formats and their applications still lag far behind the status in silicon photonics [227]. Also, it is worthwhile to note that on-chip SoC with high density and large volumes are inseparable from the direct synthesis and characterization of 2D materials on optical waveguide devices, which are also waiting for a technical breakthrough [228]. With the development of complex SoC, 2D-material OEICs could find more applications in optical communications, optical interconnects, supercomputers, quantum technology, and brain-like chips, serving as a powerful candidate for ICT development in the post-Moore era.

(5) 2D-material optoelectronic devices towards mid-IR and far-IR spectral regions are promising to explore. Compared with the visible light and telecommunication band, the development of mid-IR optoelectronic devices is still in its infancy. For example, current mid-IR photodetectors, namely, HgCdTe [229], intersubband transitions in quantum wells [230], and heterojunction superlattices [231], usually suffer from the limitations of low device operating temperature, high dark currents, and difficulties of integrating with optical waveguides. The flexible tunability of energy band gaps of 2D materials provides a broad space for improving IR device performances in this area. By integrating 2D materials with novel long-wavelength photonic integrated circuits, namely silicon/germanium suspended membrane waveguide [232–237], it is expected to bring us tremendous applications in free-space communications, imaging, remote sensing, and spectroscopy [238–240].

(6) It is promising to develop innovative sensors based on 2D-material hybrid waveguides. Besides

working as photosensitive materials, many great efforts have been made to demonstrate that 2D materials could be outstanding heat-sensitive materials [241] and gas-sensitive materials [224,242,243]. Moreover, due to the unique advantages in exciting surface plasmon polaritons in mid-IR wavelengths and THz frequencies [220,244], selective molecular adsorption and Fermi level doping features [245], and fluorescence quenching [246], 2D materials are also used for the biochemical sensitization, enabling single-molecule detection based on optical methods [247]. Consequently, 2D-material heterogeneous OEICs are potential great candidates to develop high-performance biochemical sensors.

## Acknowledgements

The authors thank Ms. W. Yang, Ms. R. Wang, Ms. X. Li, Ms. J. Wu, and Mr. C. Lin for their support on the information collections and figure preparation.

## Funding

This work was partly supported by the National Natural Science Foundation of China (62161160335, 62175179, 61922034, 61805164, 61805175), the Science and Technology Plan Project of Shenzhen (JCYJ20190808120801661), and Hong Kong Research Grants Council (RGC) Research Grants (N\_CUHK423/21).

## Author contributions

Z. Cheng, J. Wang, Y. Yu, and H.K. Tsang supervised the project. Z. Cheng, J. Wang, R. Guo, and Y. Wang organized the manuscript structure. Z. Cheng, R. Guo, J. Wang, Y. Wang, Z. Xing, L. Ma, W. Wei, Y. Yu, H.K. Tsang, and T. Liu contributed to the discussions and wrote the manuscript.

## Conflict of interest

The authors declare no conflict of interest.

## References

- 1 Hao Y, Xiang S, Han G, *et al.* Recent progress of integrated circuits and optoelectronic chips. *Sci China Inf Sci* 2021; **64**: 201401.
- 2 Wu J, Yue G, Chen W, *et al.* On-chip optical gas sensors based on group-IV materials. *ACS Photonics* 2020; **7**: 2923–2940.
- 3 Jin M, Tang SJ, Chen JH, *et al.*  $1/f$ -noise-free optical sensing with an integrated heterodyne interferometer. *Nat Commun* 2021; **12**: 1973.
- 4 Li Y, Li J, Yu H, *et al.* On-chip photonic microsystem for optical signal processing based on silicon and silicon nitride platforms. *Adv Opt Technol* 2018; **7**: 81–101.
- 5 Liu W, Li M, Guzzon RS, *et al.* A fully reconfigurable photonic integrated signal processor. *Nat Photon* 2016; **10**: 190–195.
- 6 Yang L, Ji R, Zhang L, *et al.* On-chip CMOS-compatible optical signal processor. *Opt Express* 2012; **20**: 13560.
- 7 Yang L, Zhou T, Jia H, *et al.* General architectures for on-chip optical space and mode switching. *Optica* 2018; **5**: 180–187.
- 8 Luo LW, Ophir N, Chen CP, *et al.* WDM-compatible mode-division multiplexing on a silicon chip. *Nat Commun* 2014; **5**: 3069.
- 9 Miller SE. Integrated optics: An introduction. *Bell Syst Technical J* 1969; **48**: 2059–2069.
- 10 Rahim A, Ryckeboer E, Subramanian AZ, *et al.* Expanding the silicon photonics portfolio with silicon nitride photonic

- integrated circuits. *J Lightwave Technol* 2017; **35**: 639–649.
- 11 Jalali B, Fathpour S. Silicon photonics. *J Lightwave Technol* 2006; **24**: 4600–4615.
  - 12 Cheng Z, Chen W, Liu T. *Mid-Infrared Germanium Photonics*. Bellingham: SPIE, 2020.
  - 13 Guo R, Chen W, Gao H, *et al.* Is Ge an excellent material for mid-IR Kerr frequency combs around 3- $\mu$ m wavelengths? *J Lightwave Technol* 2022; **40**: 2097–2103.
  - 14 Dietrich CP, Fiore A, Thompson MG, *et al.* GaAs integrated quantum photonics: Towards compact and multi-functional quantum photonic integrated circuits. *Laser Photonics Rev* 2016; **10**: 870–894.
  - 15 Smit MK, Williams KA. Indium phosphide photonic integrated circuits. In: Optical Fiber Communication Conference (OFC). OSA Technical Digest. San Diego, 2020.
  - 16 Qi Y, Li Y. Integrated lithium niobate photonics. *Nanophotonics* 2020; **9**: 1287–1320.
  - 17 Xu M, He M, Zhang H, *et al.* High-performance coherent optical modulators based on thin-film lithium niobate platform. *Nat Commun* 2020; **11**: 3911.
  - 18 Yan Z, Han Y, Lin L, *et al.* A monolithic InP/SOI platform for integrated photonics. *Light Sci Appl* 2021; **10**: 200.
  - 19 Roelkens G, Liu L, Liang D, *et al.* III-V/silicon photonics for on-chip and intra-chip optical interconnects. *Laser Photon Rev* 2010; **4**: 751–779.
  - 20 Han X, Jiang Y, Frigg A, *et al.* Mode and polarization-division multiplexing based on silicon nitride loaded lithium niobate on insulator platform. *Laser Photonics Rev* 2022; **16**: 2100529.
  - 21 Goyvaerts J, Grabowski A, Gustavsson J, *et al.* Enabling VCSEL-on-silicon nitride photonic integrated circuits with micro-transfer-printing. *Optica* 2021; **8**: 1573.
  - 22 Xue Y, Han Y, Tong Y, *et al.* High-performance III-V photodetectors on a monolithic InP/SOI platform. *Optica* 2021; **8**: 1204.
  - 23 Novoselov KS, Geim AK, Morozov SV, *et al.* Electric field effect in atomically thin carbon films. *Science* 2004; **306**: 666–669.
  - 24 Deilmann T, Rohlfing M, Wurstbauer U. Light-matter interaction in van der Waals hetero-structures. *J Phys-Condens Matter* 2020; **32**: 333002.
  - 25 Berger C, Song Z, Li T, *et al.* Evidence for 2D electron gas behavior in ultrathin epitaxial graphite on a SiC substrate. In: American Physical Society, March Meeting 2004. Montreal, 2004. A17.008.
  - 26 Mounet N, Gibertini M, Schwaller P, *et al.* Two-dimensional materials from high-throughput computational exfoliation of experimentally known compounds. *Nat Nanotech* 2018; **13**: 246–252.
  - 27 Bhimanapati GR, Glavin NR, Robinson JA. Chapter three: 2D boron nitride: Synthesis and applications. In: Iacopi F, J Boeckl J, Jagadish C, Eds. *Semiconductors and Semimetals*. California: Elsevier, 2016. 101.
  - 28 Manzeli S, Ovchinnikov D, Pasquier D, *et al.* 2D transition metal dichalcogenides. *Nat Rev Mater* 2017; **2**: 17033.
  - 29 Li L, Yu Y, Ye GJ, *et al.* Black phosphorus field-effect transistors. *Nat Nanotech* 2014; **9**: 372–377.
  - 30 Tao W, Kong N, Ji X, *et al.* Emerging two-dimensional mono-elemental materials (Xenes) for biomedical applications. *Chem Soc Rev* 2019; **48**: 2891–2912.
  - 31 Liu M, Yin X, Ulin-Avila E, *et al.* A graphene-based broadband optical modulator. *Nature* 2011; **474**: 64–67.
  - 32 Wallace PR. The band theory of graphite. *Phys Rev* 1947; **71**: 622–634.
  - 33 Nair RR, Blake P, Grigorenko AN, *et al.* Fine structure constant defines visual transparency of graphene. *Science* 2008; **320**: 1308.
  - 34 Bolotin KI, Sikes KJ, Jiang Z, *et al.* Ultrahigh electron mobility in suspended graphene. *Solid State Commun* 2008; **146**: 351–355.
  - 35 Zhang H, Vally S, Bao Q, *et al.* Z-scan measurement of the nonlinear refractive index of graphene. *Opt Lett* 2012; **37**: 1856.
  - 36 Zhang Y, Tang TT, Girit C, *et al.* Direct observation of a widely tunable bandgap in bilayer graphene. *Nature* 2009; **459**: 820–823.
  - 37 Liu H, Liu Y, Zhu D. Chemical doping of graphene. *J Mater Chem* 2011; **21**: 3335–3345.

- 38 Kosynkin DV, Higginbotham AL, Sinitiskii A, *et al.* Longitudinal unzipping of carbon nanotubes to form graphene nanoribbons. *Nature* 2009; **458**: 872–876.
- 39 Tran V, Soklaski R, Liang Y, *et al.* Layer-controlled band gap and anisotropic excitons in few-layer black phosphorus. *Phys Rev B* 2014; **89**: 235319.
- 40 Long G, Maryenko D, Shen J, *et al.* Achieving ultrahigh carrier mobility in two-dimensional hole gas of black phosphorus. *Nano Lett* 2016; **16**: 7768–7773.
- 41 Kim YJ, Lee Y, Kim K, *et al.* Light-induced anisotropic morphological dynamics of black phosphorus membranes visualized by dark-field ultrafast electron microscopy. *ACS Nano* 2020; **14**: 11383–11393.
- 42 Li XJ, Yu JH, Luo K, *et al.* Tuning the electrical and optical anisotropy of a monolayer black phosphorus magnetic superlattice. *Nanotechnology* 2018; **29**: 174001.
- 43 Zheng X, Chen R, Shi G, *et al.* Characterization of nonlinear properties of black phosphorus nanoplatelets with femtosecond pulsed Z-scan measurements. *Opt Lett* 2015; **40**: 3480.
- 44 Wang G, Slough WJ, Pandey R, *et al.* Degradation of phosphorene in air: Understanding at atomic level. *2D Mater* 2016; **3**: 025011.
- 45 Laxmi V, Dong W, Wang H, *et al.* Protecting black phosphorus with selectively adsorbed graphene quantum dot layers. *Appl Surf Sci* 2021; **538**: 148089.
- 46 Wang P, Yang D, Pi X. Toward wafer-scale production of 2D transition metal chalcogenides. *Adv Electron Mater* 2021; **7**: 2100278.
- 47 Keum DH, Cho S, Kim JH, *et al.* Bandgap opening in few-layered monoclinic MoTe<sub>2</sub>. *Nat Phys* 2015; **11**: 482–486.
- 48 Wang Y, Xiao J, Zhu H, *et al.* Structural phase transition in monolayer MoTe<sub>2</sub> driven by electrostatic doping. *Nature* 2017; **550**: 487–491.
- 49 Wang Y, Li L, Yao W, *et al.* Monolayer PtSe<sub>2</sub>, a new semiconducting transition-metal-dichalcogenide, epitaxially grown by direct selenization of Pt. *Nano Lett* 2015; **15**: 4013–4018.
- 50 Sun J, Shi H, Siegrist T, *et al.* Electronic, transport, and optical properties of bulk and mono-layer PdSe<sub>2</sub>. *Appl Phys Lett* 2015; **107**: 153902.
- 51 Oyedele AD, Yang S, Liang L, *et al.* PdSe<sub>2</sub>: Pentagonal two-dimensional layers with high air stability for electronics. *J Am Chem Soc* 2017; **139**: 14090–14097.
- 52 Iqbal MW, Elahi E, Amin A, *et al.* A facile route to enhance the mobility of MoTe<sub>2</sub> field effect transistor via chemical doping. *Superlattice Microstruct* 2020; **147**: 106698.
- 53 Moss D. Large and negative self-defocusing optical Kerr nonlinearity in Palladium di-Selenide 2D films. *Research Square* 2021; <https://doi.org/10.21203/rs.3.rs-537813/v1>.
- 54 Lu JP. Elastic properties of carbon nanotubes and nanoropes. *Phys Rev Lett* 1997; **79**: 1297–1300.
- 55 Castellanos-Gomez A, Vicarelli L, Prada E, *et al.* Isolation and characterization of few-layer black phosphorus. *2D Mater* 2014; **1**: 025001.
- 56 Ruppert C, Aslan OB, Heinz TF. Optical properties and band gap of single- and few-layer MoTe<sub>2</sub> crystals. *Nano Lett* 2014; **14**: 6231–6236.
- 57 Yang J, Lü T, Myint YW, *et al.* Robust excitons and trions in monolayer MoTe<sub>2</sub>. *ACS Nano* 2015; **9**: 6603–6609.
- 58 Zhao Y, Qiao J, Yu Z, *et al.* High-electron-mobility and air-stable 2D layered PtSe<sub>2</sub> FETs. *Adv Mater* 2017; **29**: 1604230.
- 59 Zhao X, Liu F, Liu D, *et al.* Thickness-dependent ultrafast nonlinear absorption properties of PtSe<sub>2</sub> films with both semiconducting and semimetallic phases. *Appl Phys Lett* 2019; **115**: 263102.
- 60 Chow WL, Yu P, Liu F, *et al.* High mobility 2D palladium diselenide field-effect transistors with tunable ambipolar characteristics. *Adv Mater* 2017; **29**: 1602969.
- 61 Zhang G, Amani M, Chaturvedi A, *et al.* Optical and electrical properties of two-dimensional palladium diselenide. *Appl Phys Lett* 2019; **114**: 253102.
- 62 Zhang J, Wang F, Shenoy VB, *et al.* Towards controlled synthesis of 2D crystals by chemical vapor deposition (CVD).

- Mater Today* 2020; **40**: 132–139.
- 63 Li G, Zhang YY, Guo H, *et al.* Epitaxial growth and physical properties of 2D materials beyond graphene: From monatomic materials to binary compounds. *Chem Soc Rev* 2018; **47**: 6073–6100.
- 64 Huo C, Yan Z, Song X, *et al.* 2D materials via liquid exfoliation: A review on fabrication and applications. *Sci Bull* 2015; **60**: 1994–2008.
- 65 Zhou D, Zhao L, Li B. Recent progress in solution assembly of 2D materials for wearable energy storage applications. *J Energy Chem* 2021; **62**: 27–42.
- 66 Mannix AJ, Kiraly B, Hersam MC, *et al.* Synthesis and chemistry of elemental 2D materials. *Nat Rev Chem* 2017; **1**: 0014.
- 67 Chen Z, Qi Y, Chen X, *et al.* Direct CVD growth of graphene on traditional glass: Methods and mechanisms. *Adv Mater* 2019; **31**: 1803639.
- 68 Berger C, Song Z, Li X, *et al.* Electronic confinement and coherence in patterned epitaxial graphene. *Science* 2006; **312**: 1191–1196.
- 69 Wang X, Cheng Z, Xu K, *et al.* High-responsivity graphene/silicon-heterostructure waveguide photodetectors. *Nat Photon* 2013; **7**: 888–891.
- 70 Wang J, Cheng Z, Chen Z, *et al.* High-responsivity graphene-on-silicon slot waveguide photodetectors. *Nanoscale* 2016; **8**: 13206–13211.
- 71 Chen K, Zhou X, Cheng X, *et al.* Graphene photonic crystal fibre with strong and tunable light-matter interaction. *Nat Photonics* 2019; **13**: 754–759.
- 72 Yu Z, Wang Y, Sun B, *et al.* Hybrid 2D-material photonics with bound states in the continuum. *Adv Opt Mater* 2019; **7**: 1901306.
- 73 Cheng Z, Tsang HK, Wang X, *et al.* In-plane optical absorption and free carrier absorption in graphene-on-silicon waveguides. *IEEE J Sel Top Quantum Electron* 2014; **20**: 43–48.
- 74 Chu R, Guan C, Bo Y, *et al.* All-optical graphene-oxide humidity sensor based on a side-polished symmetrical twin-core fiber Michelson interferometer. *Sens Actuat B-Chem* 2019; **284**: 623–627.
- 75 Ju L, Geng B, Horng J, *et al.* Graphene plasmonics for tunable terahertz metamaterials. *Nat Nanotech* 2011; **6**: 630–634.
- 76 Nematpour A, Lisi N, Piegari A, *et al.* Experimental near infrared absorption enhancement of graphene layers in an optical resonant cavity. *Nanotechnology* 2019; **30**: 445201.
- 77 Soref RA, Bennett BR. Electrooptical effects in silicon. *IEEE J Quantum Electron* 1987; **23**: 123–129.
- 78 Li H, Anugrah Y, Koester SJ, *et al.* Optical absorption in graphene integrated on silicon waveguides. *Appl Phys Lett* 2012; **101**: 111110.
- 79 Gruhler N, Benz C, Jang H, *et al.* High-quality Si<sub>3</sub>N<sub>4</sub> circuits as a platform for graphene-based nanophotonic devices. *Opt Express* 2013; **21**: 31678.
- 80 Wang J, Cheng Z, Shu C, *et al.* Optical absorption in graphene-on-silicon nitride microring resonators. *IEEE Photon Technol Lett* 2015; **27**: 1765–1767.
- 81 Wang J, Cheng Z, Xu K, *et al.* Optical absorption and thermal nonlinearities in graphene-on-silicon nitride microring resonators. In: Asia Communications and Photonics Conference. Hong Kong: OSA Technical Digest, 2015.
- 82 Kim JT, Choi CG. Graphene-based polymer waveguide polarizer. *Opt Express* 2012; **20**: 3556.
- 83 Chen B, Meng C, Yang Z, *et al.* Graphene coated ZnO nanowire optical waveguides. *Opt Express* 2014; **22**: 24276.
- 84 Lin H, Song Y, Huang Y, *et al.* Chalcogenide glass-on-graphene photonics. *Nat Photon* 2017; **11**: 798–805.
- 85 Kou R, Tanabe S, Tsuchizawa T, *et al.* Characterization of optical absorption and polarization dependence of single-layer graphene integrated on a silicon wire waveguide. *Jpn J Appl Phys* 2013; **52**: 060203.
- 86 Tan Y, He R, Cheng C, *et al.* Polarization-dependent optical absorption of MoS<sub>2</sub> for refractive index sensing. *Sci Rep* 2014; **4**: 7523.
- 87 Wei G, Stanev TK, Czaplewski DA, *et al.* Silicon-nitride photonic circuits interfaced with monolayer MoS<sub>2</sub>. *Appl Phys*

- Lett* 2015; **107**: 091112.
- 88 Gan X, Mak KF, Gao Y, *et al.* Strong enhancement of light-matter interaction in graphene coupled to a photonic crystal nanocavity. *Nano Lett* 2012; **12**: 5626–5631.
- 89 Kou R, Tanabe S, Tsuchizawa T, *et al.* Influence of graphene on quality factor variation in a silicon ring resonator. *Appl Phys Lett* 2014; **104**: 091122.
- 90 Cai H, Cheng Y, Zhang H, *et al.* Enhanced linear absorption coefficient of in-plane monolayer graphene on a silicon microring resonator. *Opt Express* 2016; **24**: 24105.
- 91 Gan X, Shiue RJ, Gao Y, *et al.* Controlled light-matter interaction in graphene electrooptic devices using nanophotonic cavities and waveguides. *IEEE J Sel Top Quantum Electron* 2014; **20**: 95–105.
- 92 Shi Z, Gan L, Xiao TH, *et al.* All-optical modulation of a graphene-cladded silicon photonic crystal cavity. *ACS Photonics* 2015; **2**: 1513–1518.
- 93 Cheng Z, Wang J, Zhu B, *et al.* Graphene absorption enhancement using silicon slot waveguides. In: 2015 IEEE Photonics Conference (IPC). Reston, 2015. 186.
- 94 Shi Z, Wong CY, Cheng Z, *et al.* In-plane saturable absorption of graphene on silicon waveguides. In: 2013 Conference on Lasers and Electro-Optics Pacific Rim. Kyoto, 2013.
- 95 Demongodin P, El Dirani H, Lhuillier J, *et al.* Ultrafast saturable absorption dynamics in hybrid graphene/Si<sub>3</sub>N<sub>4</sub> waveguides. *APL Photonics* 2019; **4**: 076102.
- 96 Wang J, Cheng Z, Xie Q, *et al.* Relaxation dynamics of optically generated carriers in graphene-on-silicon nitride waveguide devices. In: CLEO: 2015. San Jose, 2015.
- 97 Wang J, Zhang L, Chen Y, *et al.* Saturable absorption in graphene-on-waveguide devices. *Appl Phys Express* 2019; **12**: 032003.
- 98 Qin C, Jia K, Li Q, *et al.* Electrically controllable laser frequency combs in graphene-fibre microresonators. *Light Sci Appl* 2020; **9**: 185.
- 99 Cheng Z, Tsang HK, Xu K, *et al.* Spectral hole burning in silicon waveguides with a graphene layer on top. *Opt Lett* 2013; **38**: 1930.
- 100 Yu L, Zheng J, Xu Y, *et al.* Local and nonlocal optically induced transparency effects in graphene-silicon hybrid nanophotonic integrated circuits. *ACS Nano* 2014; **8**: 11386–11393.
- 101 Wang H, Yang N, Chang L, *et al.* CMOS-compatible all-optical modulator based on the saturable absorption of graphene. *Photon Res* 2020; **8**: 468.
- 102 Sun F, Xia L, Nie C, *et al.* The all-optical modulator in dielectric-loaded waveguide with graphene-silicon heterojunction structure. *Nanotechnology* 2018; **29**: 135201.
- 103 Ono M, Hata M, Tsunekawa M, *et al.* Ultrafast and energy-efficient all-optical switching with graphene-loaded deep-subwavelength plasmonic waveguides. *Nat Photonics* 2020; **14**: 37–43.
- 104 Sun F, Xia L, Nie C, *et al.* An all-optical modulator based on a graphene-plasmonic slot waveguide at 1550 nm. *Appl Phys Express* 2019; **12**: 042009.
- 105 Jiang L, Huang Q, Chiang KS. Low-power all-optical switch based on a graphene-buried polymer waveguide Mach-Zehnder interferometer. *Opt Express* 2022; **30**: 6786.
- 106 Qiu C, Zhang C, Zeng H, *et al.* High-performance graphene-on-silicon nitride all-optical switch based on a Mach-Zehnder interferometer. *J Lightwave Technol* 2021; **39**: 2099–2105.
- 107 Cheng Z, Tsang HK, Wang X, *et al.* Polarization dependent loss of graphene-on-silicon waveguides. In: 2013 IEEE Photonics Conference. Bellevue, 2013. 460.
- 108 Pei C, Yang L, Wang G, *et al.* Broadband graphene/glass hybrid waveguide polarizer. *IEEE Photon Technol Lett* 2015; **27**: 927–930.
- 109 Xing Z, Li C, Han Y, *et al.* Waveguide-integrated graphene spatial mode filters for on-chip mode-division multiplexing. *Opt Express* 2019; **27**: 19188.
- 110 Cheng Z, Li Z, Xu K, *et al.* Increase of the grating coupler bandwidth with a graphene overlay. *Appl Phys Lett* 2014;

- 104:** 111109.
- 111 Xing Z, Li C, Han Y, *et al.* Design of on-chip polarizers based on graphene-on-silicon nanowires. *Appl Phys Express* 2019; **12**: 072001.
- 112 Cheng Z, Tsang HK. Experimental demonstration of polarization-insensitive air-cladding grating couplers for silicon-on-insulator waveguides. *Opt Lett* 2014; **39**: 2206.
- 113 Wu S, Buckley S, Schaibley JR, *et al.* Monolayer semiconductor nanocavity lasers with ultralow thresholds. *Nature* 2015; **520**: 69–72.
- 114 Li H, Huang ZT, Hong KB, *et al.* Current modulation of plasmonic nanolasers by breaking reciprocity on hybrid graphene-insulator-metal platforms. *Adv Sci* 2020; **7**: 2001823.
- 115 Chen W, Guo R, Wan D, *et al.* Design of a graphene-enabled dual-mode Kerr frequency comb. *IEEE J Sel Top Quantum Electron* 2022; **28**: 1–7.
- 116 Li H, Li JH, Hong KB, *et al.* Plasmonic nanolasers enhanced by hybrid graphene-insulator-metal structures. *Nano Lett* 2019; **19**: 5017–5024.
- 117 Ye Y, Wong ZJ, Lu X, *et al.* Monolayer excitonic laser. *Nat Photon* 2015; **9**: 733–737.
- 118 Salehzadeh O, Djavid M, Tran NH, *et al.* Optically pumped two-dimensional MoS<sub>2</sub> lasers operating at room-temperature. *Nano Lett* 2015; **15**: 5302–5306.
- 119 Li Y, Zhang J, Huang D, *et al.* Room-temperature continuous-wave lasing from monolayer molybdenum ditelluride integrated with a silicon nanobeam cavity. *Nat Nanotech* 2017; **12**: 987–992.
- 120 Alexander K, Savostianova NA, Mikhailov SA, *et al.* Electrically tunable optical nonlinearities in graphene-covered silicon waveguides characterized by four-wave mixing. *ACS Photonics* 2017; **4**: 3039–3044.
- 121 Gu T, Zhou H, McMillan JF, *et al.* Coherent four-wave mixing on hybrid graphene-silicon photonic crystals. *IEEE J Sel Top Quantum Electron* 2014; **20**: 116–121.
- 122 Wu J, Yang Y, Qu Y, *et al.* 2D layered graphene oxide films integrated with micro-ring resonators for enhanced nonlinear optics. *Small* 2020; **16**: 1906563.
- 123 Qu Y, Wu J, Yang Y, *et al.* Enhanced four-wave mixing in silicon nitride waveguides integrated with 2D layered graphene oxide films. *Adv Opt Mater* 2020; **8**: 2001048.
- 124 Yang Y, Wu J, Xu X, *et al.* Invited article: Enhanced four-wave mixing in waveguides integrated with graphene oxide. *APL Photonics* 2018; **3**: 120803.
- 125 Feng Q, Cong H, Zhang B, *et al.* Enhanced optical Kerr nonlinearity of graphene/Si hybrid waveguide. *Appl Phys Lett* 2019; **114**: 071104.
- 126 Zhou H, Gu T, McMillan JF, *et al.* Enhanced four-wave mixing in graphene-silicon slow-light photonic crystal waveguides. *Appl Phys Lett* 2014; **105**: 091111.
- 127 Hu X, Long Y, Ji M, *et al.* Graphene-silicon microring resonator enhanced all-optical up and down wavelength conversion of QPSK signal. *Opt Express* 2016; **24**: 7168.
- 128 Gu T, Petrone N, McMillan JF, *et al.* Regenerative oscillation and four-wave mixing in graphene optoelectronics. *Nat Photon* 2012; **6**: 554–559.
- 129 Ji M, Cai H, Deng L, *et al.* Enhanced parametric frequency conversion in a compact silicon-graphene microring resonator. *Opt Express* 2015; **23**: 18679.
- 130 Yang Y, Xu Z, Jiang X, *et al.* High-efficiency and broadband four-wave mixing in a silicon-graphene strip waveguide with a windowed silica top layer. *Photon Res* 2018; **6**: 965.
- 131 Yao B, Huang SW, Liu Y, *et al.* Gate-tunable frequency combs in graphene-nitride microresonators. *Nature* 2018; **558**: 410–414.
- 132 Reed GT, Mashanovich G, Gardes FY, *et al.* Silicon optical modulators. *Nat Photon* 2010; **4**: 518–526.
- 133 Han JH, Boeuf F, Fujikata J, *et al.* Efficient low-loss InGaAsP/Si hybrid MOS optical modulator. *Nat Photon* 2017; **11**: 486–490.
- 134 Wang C, Zhang M, Chen X, *et al.* Integrated lithium niobate electro-optic modulators operating at CMOS-compatible

- voltages. *Nature* 2018; **562**: 101–104.
- 135 Alloatti L, Palmer R, Diebold S, *et al.* 100 GHz silicon-organic hybrid modulator. *Light Sci Appl* 2014; **3**: e173.
- 136 Kuo YH, Lee YK, Ge Y, *et al.* Quantum-confined stark effect in Ge/SiGe quantum wells on si for optical modulators. *IEEE J Sel Top Quantum Electron* 2006; **12**: 1503–1513.
- 137 Kim W, Li C, Chaves FA, *et al.* Tunable graphene-gase dual heterojunction device. *Adv Mater* 2016; **28**: 1845–1852.
- 138 Lin L, Zhang J, Su H, *et al.* Towards super-clean graphene. *Nat Commun* 2019; **10**: 1912.
- 139 Gao Y, Shiue RJ, Gan X, *et al.* High-speed electro-optic modulator integrated with graphene-boron nitride heterostructure and photonic crystal nanocavity. *Nano Lett* 2015; **15**: 2001–2005.
- 140 Phare CT, Daniel Lee YH, Cardenas J, *et al.* Graphene electro-optic modulator with 30 GHz bandwidth. *Nat Photon* 2015; **9**: 511–514.
- 141 Wang L, Meric I, Huang PY, *et al.* One-dimensional electrical contact to a two-dimensional material. *Science* 2013; **342**: 614–617.
- 142 Shen PC, Su C, Lin Y, *et al.* Ultralow contact resistance between semimetal and monolayer semiconductors. *Nature* 2021; **593**: 211–217.
- 143 Liu M, Yin X, Zhang X. Double-layer graphene optical modulator. *Nano Lett* 2012; **12**: 1482–1485.
- 144 Dalir H, Xia Y, Wang Y, *et al.* Athermal broadband graphene optical modulator with 35 GHz speed. *ACS Photonics* 2016; **3**: 1564–1568.
- 145 Hu Y, Pantouvaki M, Van Campenhout J, *et al.* Broadband 10 Gb/s operation of graphene electro-absorption modulator on silicon. *Laser Photonics Rev* 2016; **10**: 307–316.
- 146 Alessandri C, Asselberghs I, Brems S, *et al.*  $5 \times 25$  Gbit/s WDM transmitters based on passivated graphene-silicon electro-absorption modulators. *Appl Opt* 2020; **59**: 1156.
- 147 Mohsin M, Schall D, Otto M, *et al.* Graphene based low insertion loss electro-absorption modulator on SOI waveguide. *Opt Express* 2014; **22**: 15292.
- 148 Youngblood N, Anugrah Y, Ma R, *et al.* Multifunctional graphene optical modulator and photodetector integrated on silicon waveguides. *Nano Lett* 2014; **14**: 2741–2746.
- 149 Mittendorff M, Li S, Murphy TE. Graphene-based waveguide-integrated terahertz modulator. *ACS Photonics* 2017; **4**: 316–321.
- 150 Cheng Z, Zhu X, Galili M, *et al.* Double-layer graphene on photonic crystal waveguide electro-absorption modulator with 12 GHz bandwidth. *Nanophotonics* 2020; **9**: 2377–2385.
- 151 Giambra MA, Sorianello V, Miseikis V, *et al.* High-speed double layer graphene electro-absorption modulator on SOI waveguide. *Opt Express* 2019; **27**: 20145.
- 152 Lee BS, Kim B, Freitas AP, *et al.* High-performance integrated graphene electro-optic modulator at cryogenic temperature. *Nanophotonics* 2021; **10**: 99–104.
- 153 Ding Y, Zhu X, Xiao S, *et al.* Effective electro-optical modulation with high extinction ratio by a graphene-silicon microring resonator. *Nano Lett* 2015; **15**: 4393–4400.
- 154 Qiu C, Gao W, Vajtai R, *et al.* Efficient modulation of 1.55  $\mu\text{m}$  radiation with gated graphene on a silicon microring resonator. *Nano Lett* 2014; **14**: 6811–6815.
- 155 Phatak A, Cheng Z, Qin C, *et al.* Design of electro-optic modulators based on graphene-on-silicon slot waveguides. *Opt Lett* 2016; **41**: 2501.
- 156 Ansell D, Radko IP, Han Z, *et al.* Hybrid graphene plasmonic waveguide modulators. *Nat Commun* 2015; **6**: 8846.
- 157 Ding Y, Guan X, Zhu X, *et al.* Efficient electro-optic modulation in low-loss graphene-plasmonic slot waveguides. *Nanoscale* 2017; **9**: 15576–15581.
- 158 Hao R, Jiao J, Peng X, *et al.* Experimental demonstration of a graphene-based hybrid plasmonic modulator. *Opt Lett* 2019; **44**: 2586.
- 159 Sorianello V, Midrio M, Contestabile G, *et al.* Graphene-silicon phase modulators with gigahertz bandwidth. *Nat Photon* 2018; **12**: 40–44.

- 160 Mohsin M, Neumaier D, Schall D, *et al.* Experimental verification of electro-refractive phase modulation in graphene. *Sci Rep* 2015; **5**: 10967.
- 161 Shu H, Su Z, Huang L, *et al.* Significantly high modulation efficiency of compact graphene modulator based on silicon waveguide. *Sci Rep* 2018; **8**: 991.
- 162 Mao D, Cheng C, Wang F, *et al.* Device architectures for low voltage and ultrafast graphene integrated phase modulators. *IEEE J Sel Top Quantum Electron* 2021; **27**: 1–9.
- 163 Yue G, Xing Z, Hu H, *et al.* Graphene-based dual-mode modulators. *Opt Express* 2020; **28**: 18456.
- 164 Wang J, Qiu H, Wei Z, *et al.* Design of a graphene-based waveguide-integrated multimode phase modulator. *IEEE Photonics J* 2021; **13**: 1–6.
- 165 Yan S, Zhu X, Frandsen LH, *et al.* Slow-light-enhanced energy efficiency for graphene microheaters on silicon photonic crystal waveguides. *Nat Commun* 2017; **8**: 14411.
- 166 Gan S, Cheng C, Zhan Y, *et al.* A highly efficient thermo-optic microring modulator assisted by graphene. *Nanoscale* 2015; **7**: 20249–20255.
- 167 Yu T, Wang F, Xu Y, *et al.* Graphene coupled with silicon quantum dots for high-performance bulk-silicon-based schottky-junction photodetectors. *Adv Mater* 2016; **28**: 4912–4919.
- 168 Hu M, Yan Y, Huang K, *et al.* Performance improvement of graphene/silicon photodetectors using high work function metal nanoparticles with plasma effect. *Adv Opt Mater* 2018; **6**: 1701243.
- 169 Koppens FHL, Mueller T, Avouris P, *et al.* Photodetectors based on graphene, other two-dimensional materials and hybrid systems. *Nat Nanotech* 2014; **9**: 780–793.
- 170 Marconi S, Giambra MA, Montanaro A, *et al.* Photo thermal effect graphene detector featuring 105 Gbit s<sup>-1</sup> NRZ and 120 Gbit s<sup>-1</sup> PAM4 direct detection. *Nat Commun* 2021; **12**: 806.
- 171 Wang Y, Yin W, Han Q, *et al.* Bolometric effect in a waveguide-integrated graphene photodetector. *Chin Phys B* 2016; **25**: 118103.
- 172 Gan X, Shiue RJ, Gao Y, *et al.* Chip-integrated ultrafast graphene photodetector with high responsivity. *Nat Photon* 2013; **7**: 883–887.
- 173 Pospischil A, Humer M, Furchi MM, *et al.* CMOS-compatible graphene photodetector covering all optical communication bands. *Nat Photon* 2013; **7**: 892–896.
- 174 Cheng Z, Chen X, Wong CY, *et al.* Mid-infrared suspended membrane waveguide and ring resonator on silicon-on-insulator. *IEEE Photonics J* 2012; **4**: 1510–1519.
- 175 Palmer J, Kunc J, Hu Y, *et al.* Controlled epitaxial graphene growth within removable amorphous carbon corrals. *Appl Phys Lett* 2014; **105**: 023106.
- 176 Deokar G, Avila J, Razado-Colambo I, *et al.* Towards high quality CVD graphene growth and transfer. *Carbon* 2015; **89**: 82–92.
- 177 Schall D, Neumaier D, Mohsin M, *et al.* 50 GBit/s photodetectors based on wafer-scale graphene for integrated silicon photonic communication systems. *ACS Photonics* 2014; **1**: 781–784.
- 178 Goykhman I, Sassi U, Desiatov B, *et al.* On-chip integrated, silicon-graphene plasmonic schottky photodetector with high responsivity and avalanche photogain. *Nano Lett* 2016; **16**: 3005–3013.
- 179 Gao Y, Zhou G, Zhao N, *et al.* High-performance chemical vapor deposited graphene-on-silicon nitride waveguide photodetectors. *Opt Lett* 2018; **43**: 1399.
- 180 Gao Y, Tao L, Tsang HK, *et al.* Graphene-on-silicon nitride waveguide photodetector with interdigital contacts. *Appl Phys Lett* 2018; **112**: 211107.
- 181 Schall D, Porschatis C, Otto M, *et al.* Graphene photodetectors with a bandwidth >76 GHz fabricated in a 6" wafer process line. *J Phys D-Appl Phys* 2017; **50**: 124004.
- 182 Schuler S, Schall D, Neumaier D, *et al.* Controlled generation of a p-n junction in a waveguide integrated graphene photodetector. *Nano Lett* 2016; **16**: 7107–7112.
- 183 Li J, Yin Y, Guo J, *et al.* Hybrid ultrathin-silicon/graphene waveguide photodetector with a loop mirror reflector. *Opt*

- Express* 2020; **28**: 10725.
- 184 Zhou H, Gu T, McMillan JF, *et al.* Enhanced photoresponsivity in graphene-silicon slow-light photonic crystal waveguides. *Appl Phys Lett* 2016; **108**: 111106.
- 185 Schuler S, Schall D, Neumaier D, *et al.* Graphene photodetector integrated on a photonic crystal defect waveguide. *ACS Photonics* 2018; **5**: 4758–4763.
- 186 Wang Y, Zhang Y, Jiang Z, *et al.* Ultra-compact high-speed polarization division multiplexing optical receiving chip enabled by graphene-on-plasmonic slot waveguide photodetectors. *Adv Opt Mater* 2021; **9**: 2001215.
- 187 Guo J, Li J, Liu C, *et al.* High-performance silicon-graphene hybrid plasmonic waveguide photodetectors beyond 1.55  $\mu\text{m}$ . *Light Sci Appl* 2020; **9**: 29.
- 188 Ma P, Salamin Y, Baeuerle B, *et al.* Plasmonically enhanced graphene photodetector featuring 100 Gbit/s data reception, high responsivity, and compact size. *ACS Photonics* 2019; **6**: 154–161.
- 189 Wang G, Dai T, Lv Z, *et al.* Integrated high responsivity photodetectors based on graphene/glass hybrid waveguide. *Opt Lett* 2016; **41**: 4214.
- 190 Wang J, Cheng Z, Chen Z, *et al.* Graphene photodetector integrated on silicon nitride waveguide. *J Appl Phys* 2015; **117**: 144504.
- 191 Mišeikis V, Marconi S, Giambra MA, *et al.* Ultrafast, zero-bias, graphene photodetectors with polymeric gate dielectric on passive photonic waveguides. *ACS Nano* 2020; **14**: 11190–11204.
- 192 Wang J, Cheng Z, Zhu B, *et al.* Photoresponse of graphene-on-silicon nitride microring resonator. In: Conference on Lasers and Electro-Optics. San Jose, 2016.
- 193 Wang Y, Li X, Jiang Z, *et al.* Ultrahigh-speed graphene-based optical coherent receiver. *Nat Commun* 2021; **12**: 5076.
- 194 Lischke S, Peczek A, Morgan JS, *et al.* Ultra-fast germanium photodiode with 3-dB bandwidth of 265 GHz. *Nat Photon* 2021; **15**: 925–931.
- 195 Rouvalis E, Chtioui M, van Dijk F, *et al.* 170 GHz uni-traveling carrier photodiodes for InP-based photonic integrated circuits. *Opt Express* 2012; **20**: 20090.
- 196 Youngblood N, Chen C, Koester SJ, *et al.* Waveguide-integrated black phosphorus photodetector with high responsivity and low dark current. *Nat Photon* 2015; **9**: 247–252.
- 197 Chen C, Youngblood N, Peng R, *et al.* Three-dimensional integration of black phosphorus photodetector with silicon photonics and nanoplasmonics. *Nano Lett* 2017; **17**: 985–991.
- 198 Huang L, Dong B, Guo X, *et al.* Waveguide-integrated black phosphorus photodetector for mid-infrared applications. *ACS Nano* 2019; **13**: 913–921.
- 199 Yin Y, Cao R, Guo J, *et al.* High-speed and high-responsivity hybrid silicon/black-phosphorus waveguide photodetectors at 2  $\mu\text{m}$ . *Laser Photonics Rev* 2019; : 1900032.
- 200 Wang Y, Yu Z, Zhang Z, *et al.* Bound-states-in-continuum hybrid integration of 2D platinum diselenide on silicon nitride for high-speed photodetectors. *ACS Photonics* 2020; **7**: 2643–2649.
- 201 Yang C, Qin S, Zuo Y, *et al.* Waveguide Schottky photodetector with tunable barrier based on  $\text{Ti}_3\text{C}_2\text{T}_x/\text{p-Si}$  van der Waals heterojunction. *Nanophotonics* 2021; **10**: 4133–4139.
- 202 Wu Z, Zhang T, Chen Y, *et al.* Integrating graphene/MoS<sub>2</sub> heterostructure with SiN<sub>x</sub> waveguide for visible light detection at 532 nm wavelength. *Phys Status Solidi RRL* 2019; **13**: 1800338.
- 203 Flöry N, Ma P, Salamin Y, *et al.* Waveguide-integrated van der Waals heterostructure photodetector at telecom wavelengths with high speed and high responsivity. *Nat Nanotechnol* 2020; **15**: 118–124.
- 204 Shiue RJ, Gao Y, Wang Y, *et al.* High-responsivity graphene-boron nitride photodetector and autocorrelator in a silicon photonic integrated circuit. *Nano Lett* 2015; **15**: 7288–7293.
- 205 Gao Y, Zhou G, Tsang HK, *et al.* High-speed van der Waals heterostructure tunneling photodiodes integrated on silicon nitride waveguides. *Optica* 2019; **6**: 514.
- 206 Gao Y, Tsang HK, Shu C. A silicon nitride waveguide-integrated chemical vapor deposited graphene photodetector with 38 GHz bandwidth. *Nanoscale* 2018; **10**: 21851–21856.

- 207 Ma Z, Kikunaga K, Wang H, *et al.* Compact graphene plasmonic slot photodetector on silicon-on-insulator with high responsivity. *ACS Photonics* 2020; **7**: 932–940.
- 208 Li G, Yoon KY, Zhong X, *et al.* A modular synthetic approach for band-gap engineering of armchair graphene nanoribbons. *Nat Commun* 2018; **9**: 1687.
- 209 Li X, Tao L, Chen Z, *et al.* Graphene and related two-dimensional materials: Structure-property relationships for electronics and optoelectronics. *Appl Phys Rev* 2017; **4**: 021306.
- 210 Guo H, Hu Z, Liu ZB, *et al.* Stacking of 2D materials. *Adv Funct Mater* 2021; **31**: 2007810.
- 211 Cao Y, Fatemi V, Fang S, *et al.* Unconventional superconductivity in magic-angle graphene superlattices. *Nature* 2018; **556**: 43–50.
- 212 Tanoh AOA, Gauriot N, Delport G, *et al.* Directed energy transfer from monolayer WS<sub>2</sub> to near-infrared emitting PbS-CdS quantum dots. *ACS Nano* 2020; **14**: 15374–15384.
- 213 Huo N, Gupta S, Konstantatos G. MoS<sub>2</sub>-HgTe quantum dot hybrid photodetectors beyond 2 μm. *Adv Mater* 2017; **29**: 1606576.
- 214 Zhang Y, Li Y, Sun J, *et al.* A micro broadband photodetector based on single wall carbon nanotubes-graphene heterojunction. *J Lightwave Technol* 2022; **40**: 149–155.
- 215 Konstantatos G, Badioli M, Gaudreau L, *et al.* Hybrid graphene-quantum dot phototransistors with ultrahigh gain. *Nat Nanotech* 2012; **7**: 363–368.
- 216 Ahn GH, Amani M, Rasool H, *et al.* Strain-engineered growth of two-dimensional materials. *Nat Commun* 2017; **8**: 608.
- 217 Dai Z, Liu L, Zhang Z. Strain engineering of 2D materials: Issues and opportunities at the interface. *Adv Mater* 2019; **31**: 1805417.
- 218 Yao B, Yu C, Wu Y, *et al.* Graphene-enhanced brillouin optomechanical microresonator for ultrasensitive gas detection. *Nano Lett* 2017; **17**: 4996–5002.
- 219 Tan T, Yuan Z, Zhang H, *et al.* Multispecies and individual gas molecule detection using Stokes solitons in a graphene over-modal microresonator. *Nat Commun* 2021; **12**: 6716.
- 220 Saeed M, Ghaffar A, Rehman S, *et al.* Graphene-based plasmonic waveguides: A mini review. *Plasmonics* 2022; **17**: 901–911.
- 221 Zhou W, Cheng Z, Chen X, *et al.* Subwavelength engineering in silicon photonic devices. *IEEE J Sel Top Quantum Electron* 2019; **25**: 1–13.
- 222 Nong J, Tang L, Lan G, *et al.* Enhanced graphene plasmonic mode energy for highly sensitive molecular fingerprint retrieval. *Laser Photonics Rev* 2021; **15**: 2000300.
- 223 Xiao TH, Cheng Z, Goda K. Graphene-on-silicon hybrid plasmonic-photonic integrated circuits. *Nanotechnology* 2017; **28**: 245201.
- 224 Cheng Z, Goda K. Design of waveguide-integrated graphene devices for photonic gas sensing. *Nanotechnology* 2016; **27**: 505206.
- 225 Yao B, Liu Y, Huang SW, *et al.* Broadband gate-tunable terahertz plasmons in graphene heterostructures. *Nat Photon* 2018; **12**: 22–28.
- 226 Li Y, An N, Lv Z, *et al.* Nonlinear co-generation of graphene plasmons for optoelectronic logic gates. *Research Square* 2022; <https://doi.org/10.21203/rs.3.rs-1204181/v1>.
- 227 Bernabé S, Wilmart Q, Hasharoni K, *et al.* Silicon photonics for terabit/s communication in data centers and exascale computers. *Solid-State Electron* 2021; **179**: 107928.
- 228 Khan A, Islam SM, Ahmed S, *et al.* Direct CVD growth of graphene on technologically important dielectric and semiconducting substrates. *Adv Sci* 2018; **5**: 1800050.
- 229 Rogalski A. HgCdTe infrared detector material: History, status and outlook. *Rep Prog Phys* 2005; **68**: 2267–2336.
- 230 Li H, Alradhi H, Jin Z, *et al.* Novel type-II InAs/AlSb core-shell nanowires and their enhanced negative photocurrent for efficient photodetection. *Adv Funct Mater* 2018; **28**: 1705382.

- 231 Li J, Dehzangi A, Razeghi M. Performance analysis of infrared heterojunction phototransistors based on Type-II superlattices. *Infrared Phys Tech* 2021; **113**: 103641.
- 232 Chen W, Wu J, Wan D, *et al.* Grating couplers beyond silicon TPA wavelengths based on MPW. *J Phys D-Appl Phys* 2021; **55**: 015109.
- 233 Kang J, Cheng Z, Zhou W, *et al.* Focusing subwavelength grating coupler for mid-infrared suspended membrane germanium waveguides. *Opt Lett* 2017; **42**: 2094.
- 234 Cheng Z, Chen X, Wong CY, *et al.* Focusing subwavelength grating coupler for mid-infrared suspended membrane waveguide. *Opt Lett* 2012; **37**: 1217.
- 235 Guo R, Gao H, Liu T, *et al.* Ultra-thin mid-infrared silicon grating coupler. *Opt Lett* 2022; **47**: 1226.
- 236 Xiao TH, Zhao Z, Zhou W, *et al.* High-Q germanium optical nanocavity. *Photon Res* 2018; **6**: 925.
- 237 Xiao TH, Zhao Z, Zhou W, *et al.* Mid-infrared high-Q germanium microring resonator. *Opt Lett* 2018; **43**: 2885.
- 238 Nong J, Tang L, Lan G, *et al.* Combined visible plasmons of ag nanoparticles and infrared plasmons of graphene nanoribbons for high-performance surface-enhanced raman and infrared spectroscopies. *Small* 2021; **17**: 2004640.
- 239 Wang L, Han L, Guo W, *et al.* Hybrid Dirac semimetal-based photodetector with efficient low-energy photon harvesting. *Light Sci Appl* 2022; **11**: 53.
- 240 He Q, Wang Y, Chen W, *et al.* Advances in short-wavelength mid-infrared silicon photonics. *Infrared Laser Eng*, 2022; **51**: 20220043.
- 241 Zuo Y, Gao Y, Qin S, *et al.* Broadband multi-wavelength optical sensing based on photothermal effect of 2D MXene films. *Nanophotonics* 2020; **9**: 123–131.
- 242 Han S, Chen W, Hu H, *et al.* Characterization method of a mid-infrared graphene-on-silicon microring with a monochromatic laser. *J Opt Soc Am B* 2020; **37**: 1683.
- 243 Wang J, Zhang X, Wei Z, *et al.* Design of a dual-mode graphene-on-microring resonator for optical gas sensing. *IEEE Access* 2021; **9**: 56479–56485.
- 244 Li Y, Li Z, Chi C, *et al.* Plasmonics of 2D nanomaterials: Properties and applications. *Adv Sci* 2017; **4**: 1600430.
- 245 Schedin F, Geim AK, Morozov SV, *et al.* Detection of individual gas molecules adsorbed on graphene. *Nat Mater* 2007; **6**: 652–655.
- 246 Zhang E, Xing Z, Wan D, *et al.* Surface-enhanced Raman spectroscopy chips based on two-dimensional materials beyond graphene. *J Semicond* 2021; **42**: 051001.
- 247 Oh SH, Altug H, Jin X, *et al.* Nanophotonic biosensors harnessing van der Waals materials. *Nat Commun* 2021; **12**: 3824.